# UFS Lecture 14: Passive Modelocking

## 7 Mode-Locking using Artificial Fast Sat. Absorbers

### 7.1.4 The Kerr Lensing Effects

### 7.2 Additive Pulse Mode-Locking

## 6 Passive Mode Locking

### 6.3 Soliton Mode Locking

## 8 Semiconductor Saturable Absorbers

### 8.1 Carrier Dynamics and Saturation Properties

### 8.2 High Fluence Effects

### 8.3 Break-up into Multiple Pulses

# 7. Mode locking using artificial fast SA
## 7.1 Kerr-lens mode locking

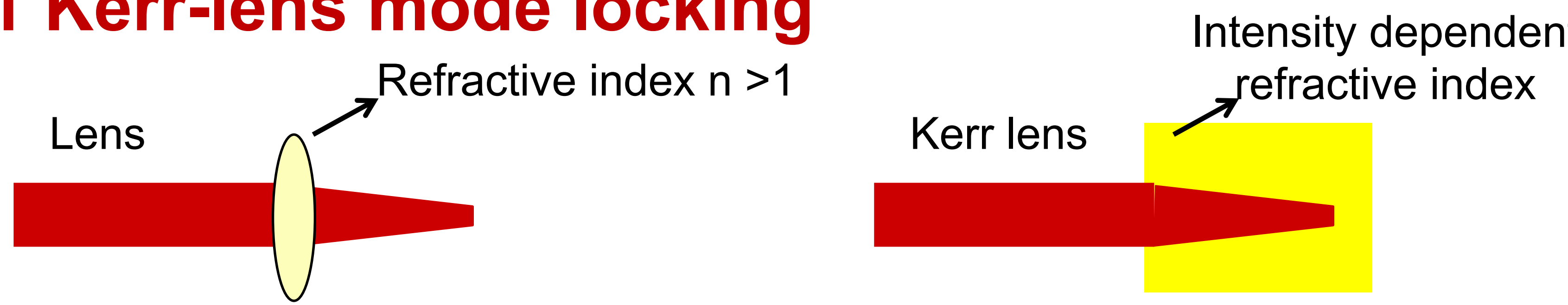


- A spatio-temporal laser pulse propagating through the Kerr medium has a time dependent mode size: pulse peak corresponds to smaller beam size than the wings.
- A hard aperture placed at the right position in the cavity strips of the wings of the pulse, shortening the pulse.
- The combined mechanism is equivalent to a fast saturable absorber.

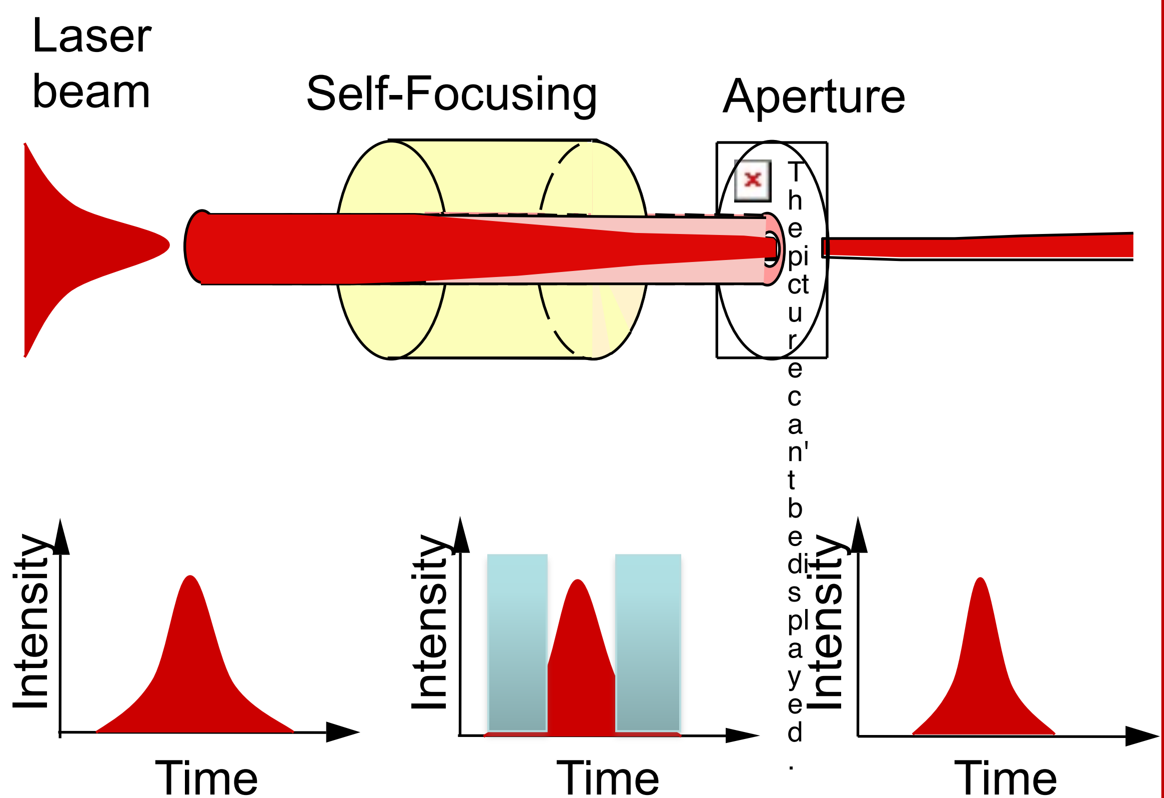

# Kerr-lens mode locking: hard aperture versus soft aperture

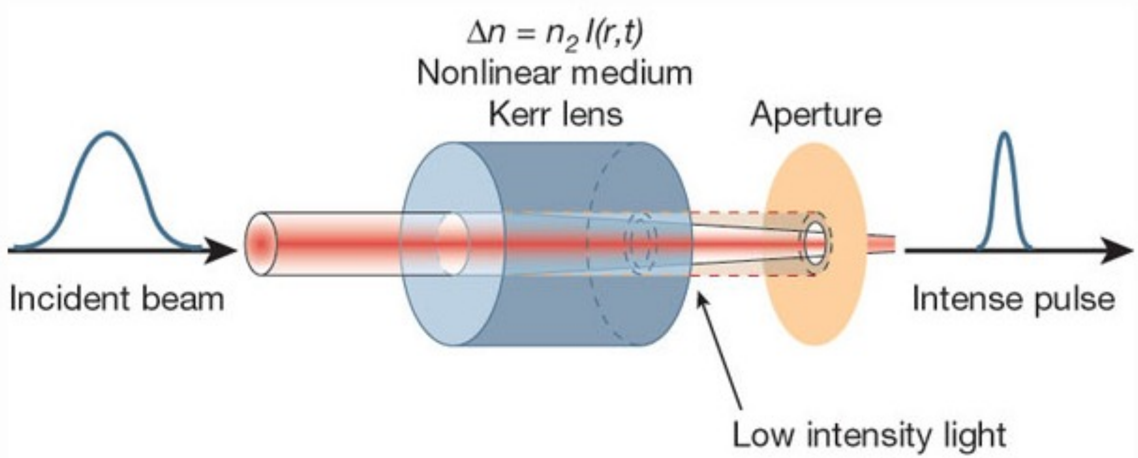


**<u>Hard-aperture Kerr-lens mode-locking</u>**: a hard aperture placed at the right position in the cavity attenuates the wings of the pulse, shortening the pulse.

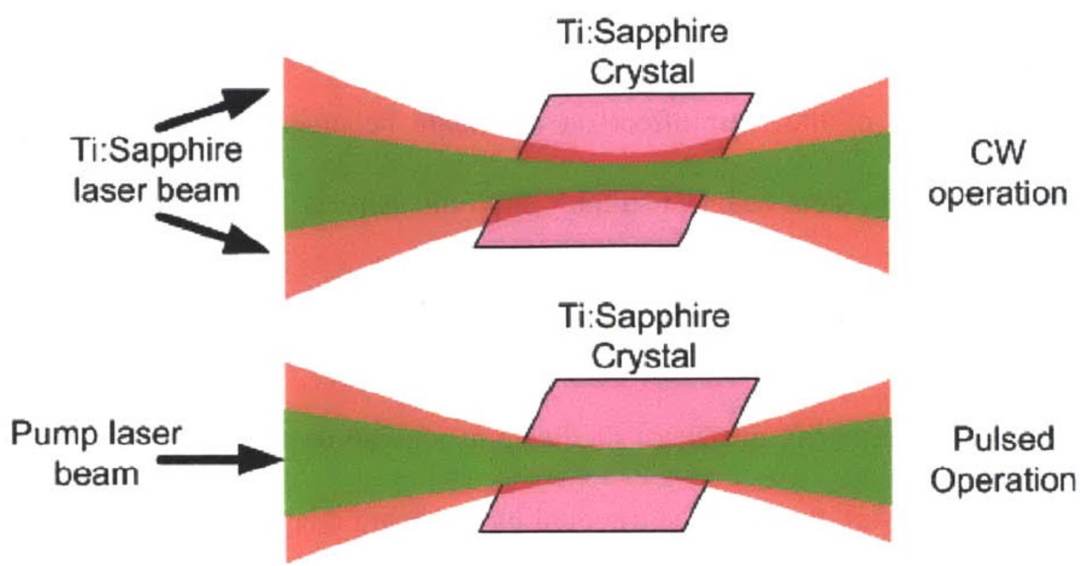


**<u>Soft-aperture Kerr-lens mode-locking</u>**: gain medium can act both as a Kerr medium and as a soft aperture (i.e. increased gain instead of saturable absorption). In the CW case the overlap between the pump beam and laser beam is poor, and the mode intensity is not high enough to utilize all of the available gain. The additional focusing provided by the high intensity pulse improves the overlap, utilizing more of the available gain.

# 7.1.4 The Kerr Lensing Effect

$$n = n_0 + n_2 I \qquad I(r) = \frac{2P}{\pi w^2}\exp\left[-2\left(\frac{r}{w}\right)^2\right]$$

$$n(r) = n_0'\left(1 - \frac{1}{2}\gamma^2 r^2\right), \text{ where}$$

$$n_0' = n_0 + n_2\frac{2P}{\pi w^2}, \; \gamma = \frac{1}{w^2}\sqrt{\frac{8n_2P}{n_0'\pi}}.$$

## Thin Lens → Gaussian Duct

| Optical Element | ABCD-Matrix |
|---|---|
| Kerr Medium Normal Incidence | $M_K = \begin{pmatrix} \cos\gamma t & \frac{1}{n_0'\gamma}\sin\gamma t \\ -n_0'\gamma\sin\gamma t & \cos\gamma t \end{pmatrix}$ |
| Kerr Medium Sagittal Plane | $M_{Ks} = \begin{pmatrix} \cos\gamma_s t & \frac{1}{n_0'\gamma_s}\sin\gamma_s t \\ -n_0'\gamma_s\sin\gamma_s t & \cos\gamma_s t \end{pmatrix}$ |
| Kerr Medium Tangential Plane | $M_{Kt} = \begin{pmatrix} \cos\gamma_t t & \frac{1}{n_0'^3\gamma_t}\sin\gamma_t t \\ -n_0'^3\gamma_t\sin\gamma_t t & \cos\gamma_t t \end{pmatrix}$ |

$$\gamma_s = \frac{1}{w_s w_t}\sqrt{\frac{8n_2P}{n_0'\pi}}$$

$$\gamma_t = \frac{1}{w_s w_t}\sqrt{\frac{8n_2P}{n_0'\pi}}$$

Table 7.2: ABCD matrices for Kerr media

$$\delta_{s,t} = \frac{1}{p}\frac{w_{s,t}(P,z) - w_{s,t}(P=0,z)}{w_{s,t}(P=0,z)}$$

$$p = P/P_{crit}, \text{ with } P_{crit} = \lambda_L^2/\left(2\pi n_2 n_0^2\right)$$

$R_1 = R_2 = 10$ cm $L_1 = 104$ cm, $L_2 = 86$ cm, $t = 2$ mm, $n = 1.76$ and $P = 200$ kW.

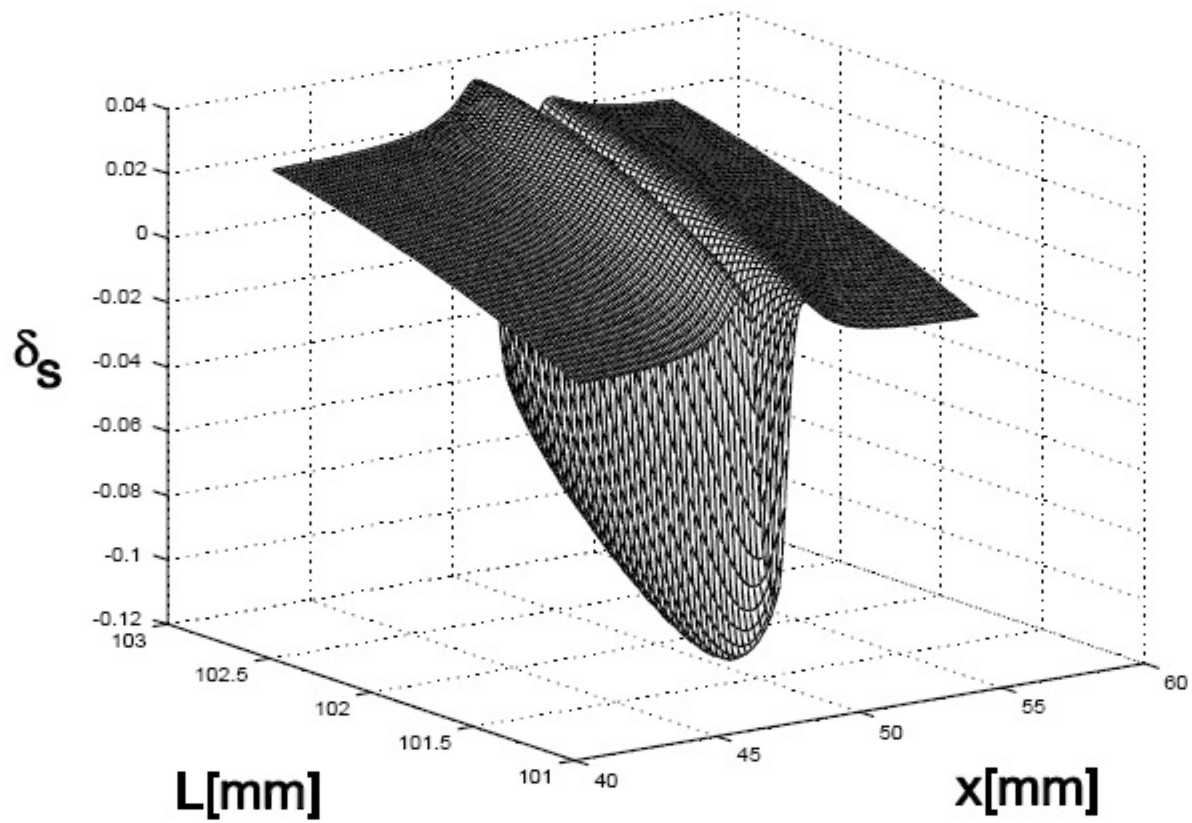


Fig. 7.15: Beam narrowing ratio

$$g \sim \int_0^\infty N(r) * N_P(r) r dr \sim \int_0^\infty \frac{2P_P}{\pi w_P^2} \exp\left[-\frac{2r^2}{w_P^2}\right] \frac{2}{\pi w_L^2} \exp\left[-\frac{2r^2}{w_L^2}\right] r dr$$

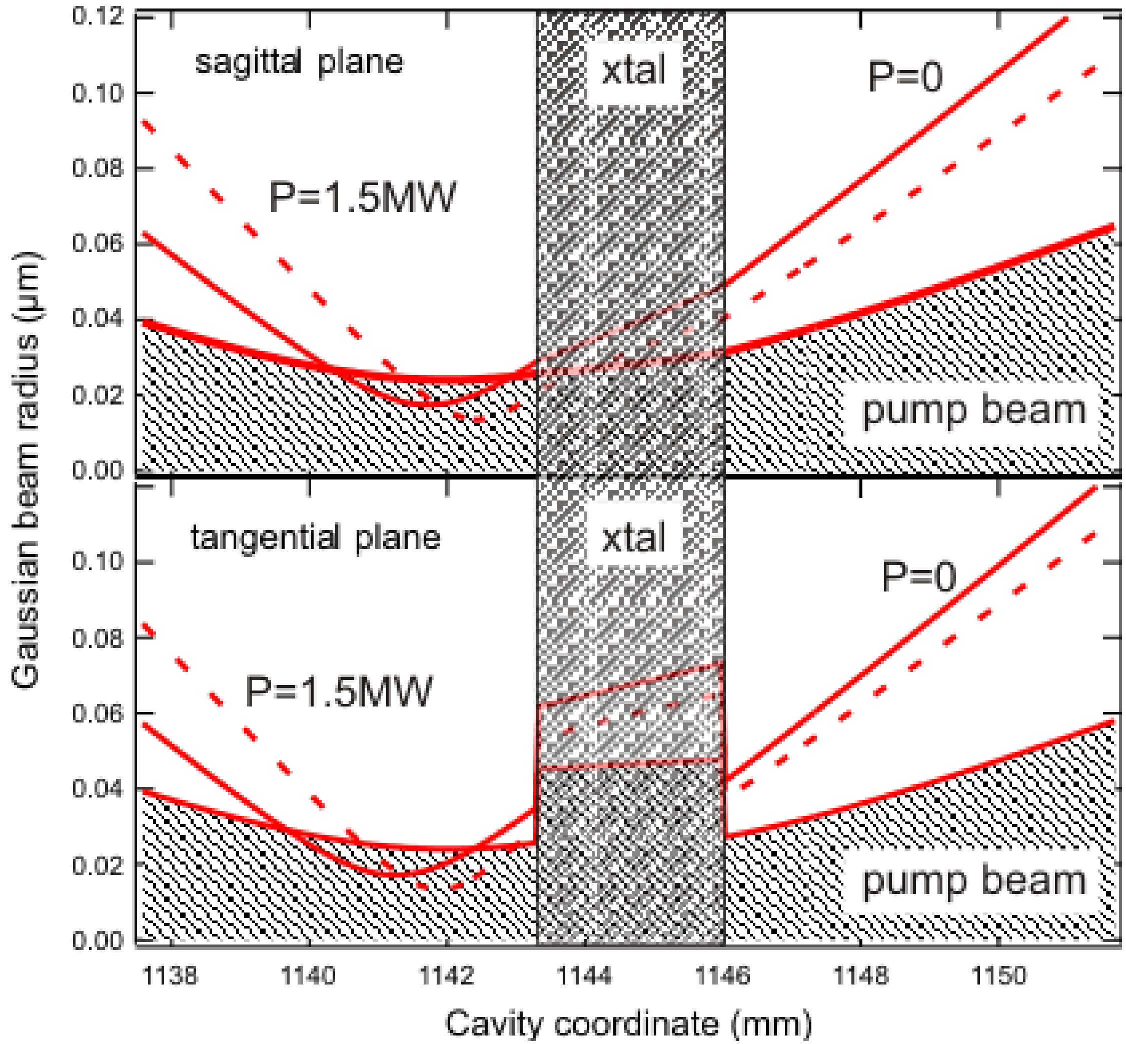


Fig. 7.16: Soft aperture KLM

# Evolution of shortest pulse duration

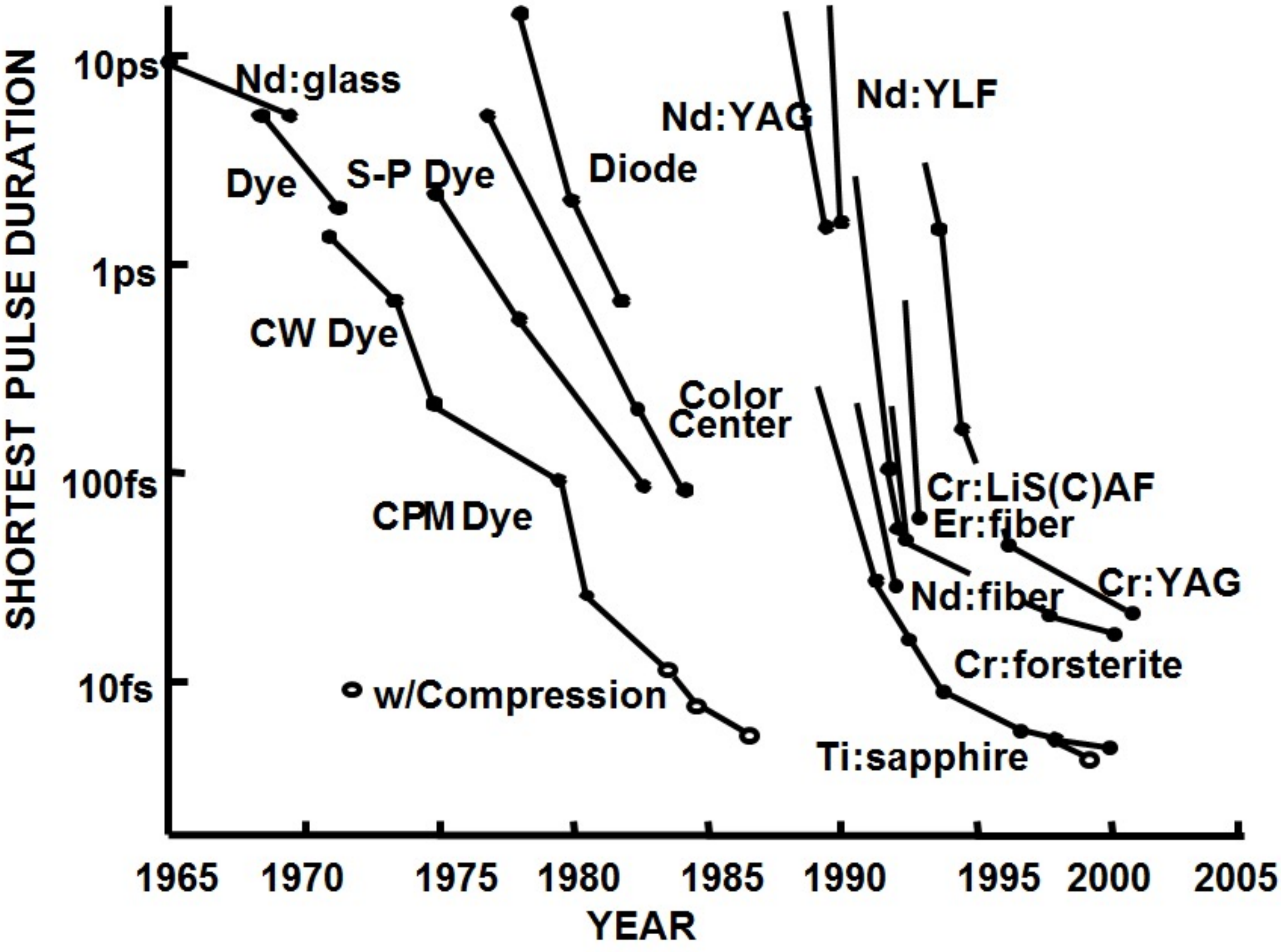

# 7 Kerr-Lens and Additive Pulse Mode Locking
## 7.2 Additive Pulse Mode Locking

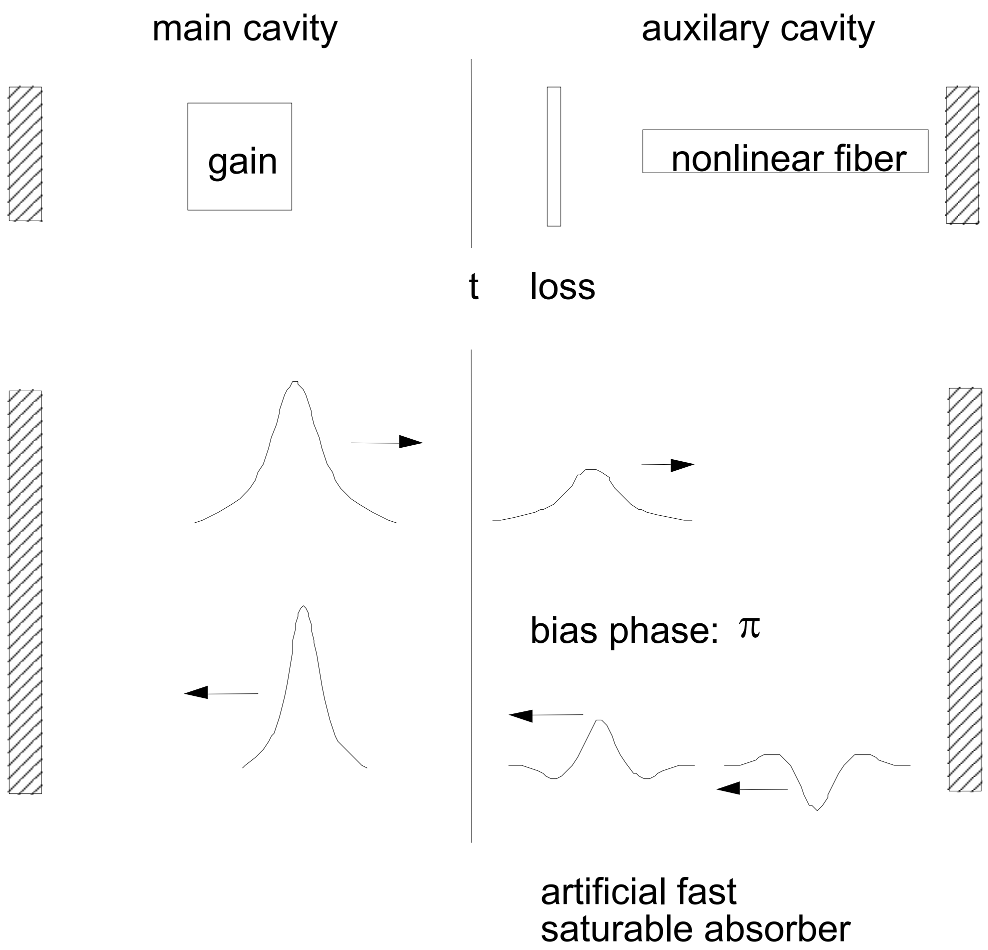


Fig. 7.17: Principle mechanism of APM

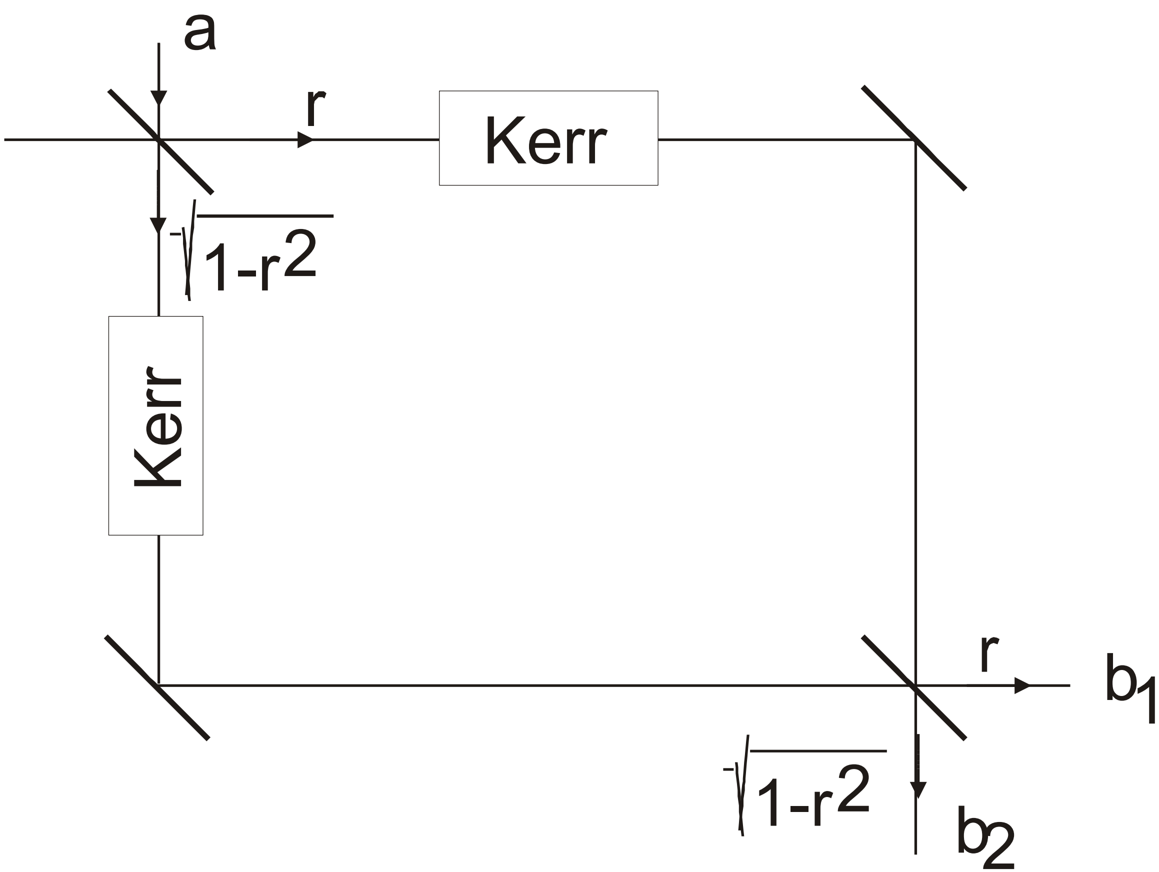


Fig. 7.18: Noninear Mach-Zehnder Interferometer

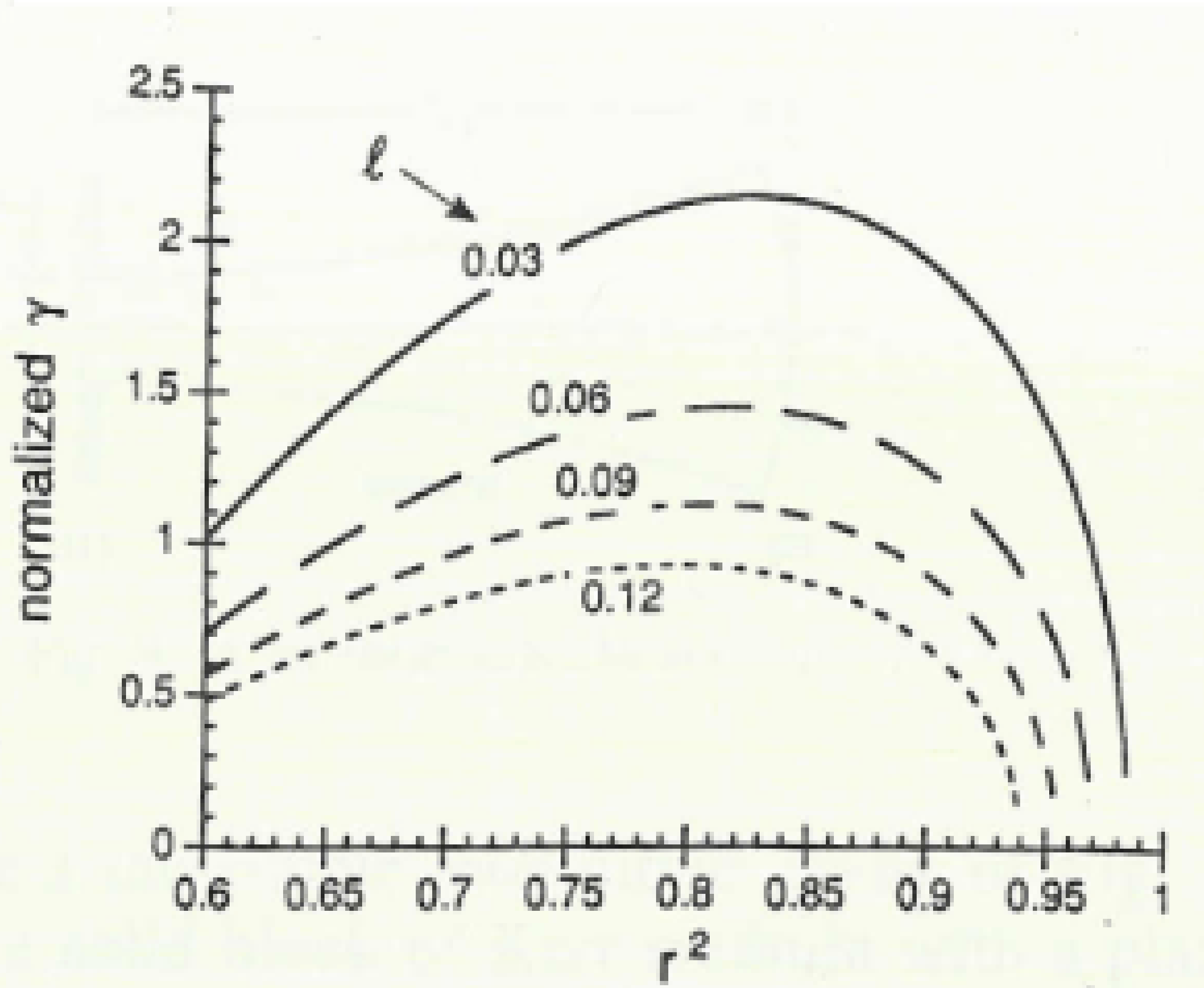


Figure 7.20: Normalized saturable absorber coefficient $\gamma / \left[ \left( \frac{2\pi}{\lambda} \right) \frac{n_2}{A_{eff}} L_{Kerr}\, l \right]$ as a function of $r^2$ with loss $l$ as parameter [25].

# 7.2 Additive pulse mode locking using nonlinear polarization rotation in a fiber

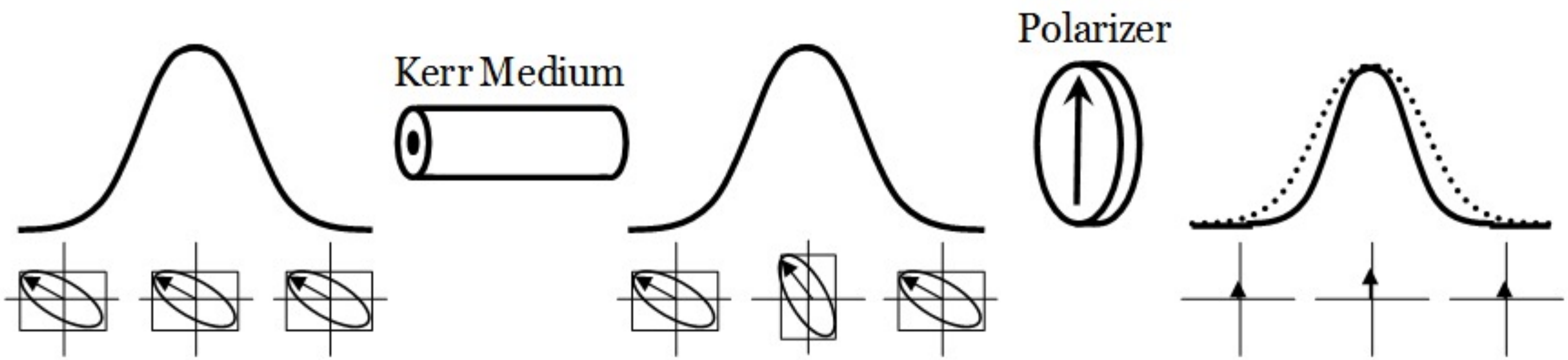


- When an intense optical pulse travels in an isotropic optical fiber, intensity-dependent change of the polarization state can happen.
- The polarization state of the pulse peak differs from that of the pulse wings after the fiber section due to Kerr effect.
- If a polarizer is placed after the fiber section and is aligned with the polarization state of the pulse peak, the pulse wings are attenuated more by the polarizer and the pulse becomes shorter.

# 200 MHz Soliton Er-fiber Laser modelocked by APM

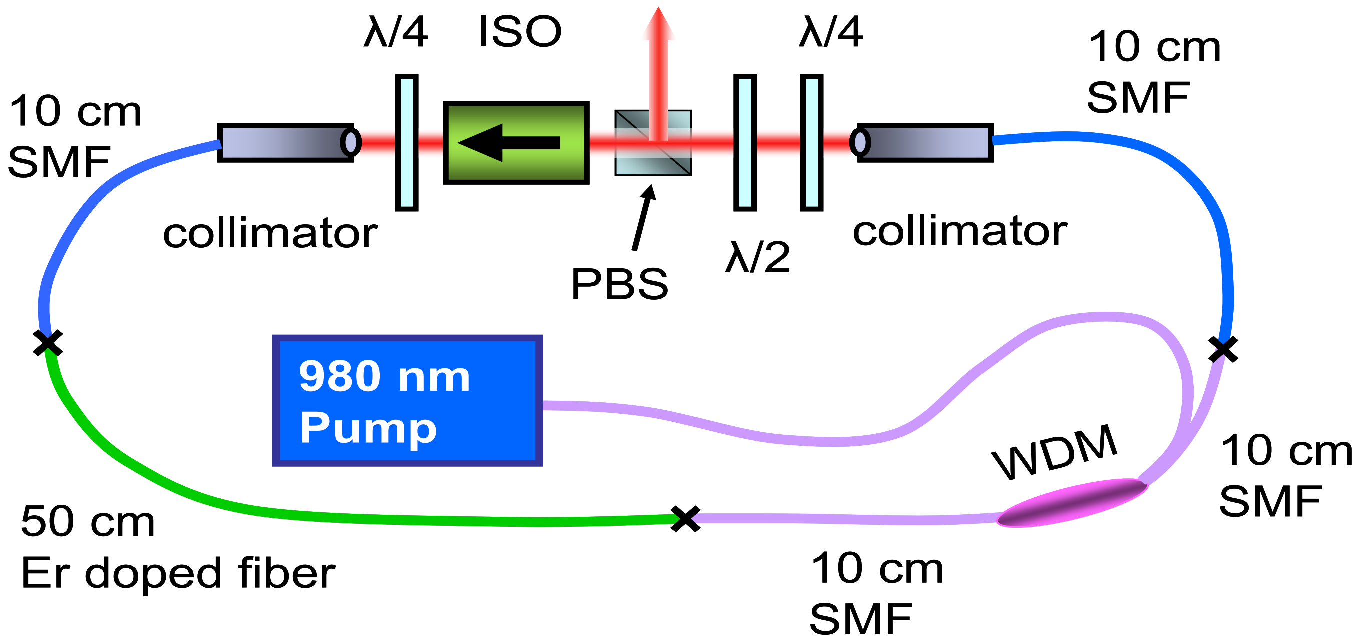


- 167 fs pulses
- 200 pJ intracavity pulse energy
- 200 pJ output pulse energy

K. Tamura et al. Opt. Lett. 18, 1080 (1993).
J. Chen et al, Opt. Lett. 32, 1566 (2007).

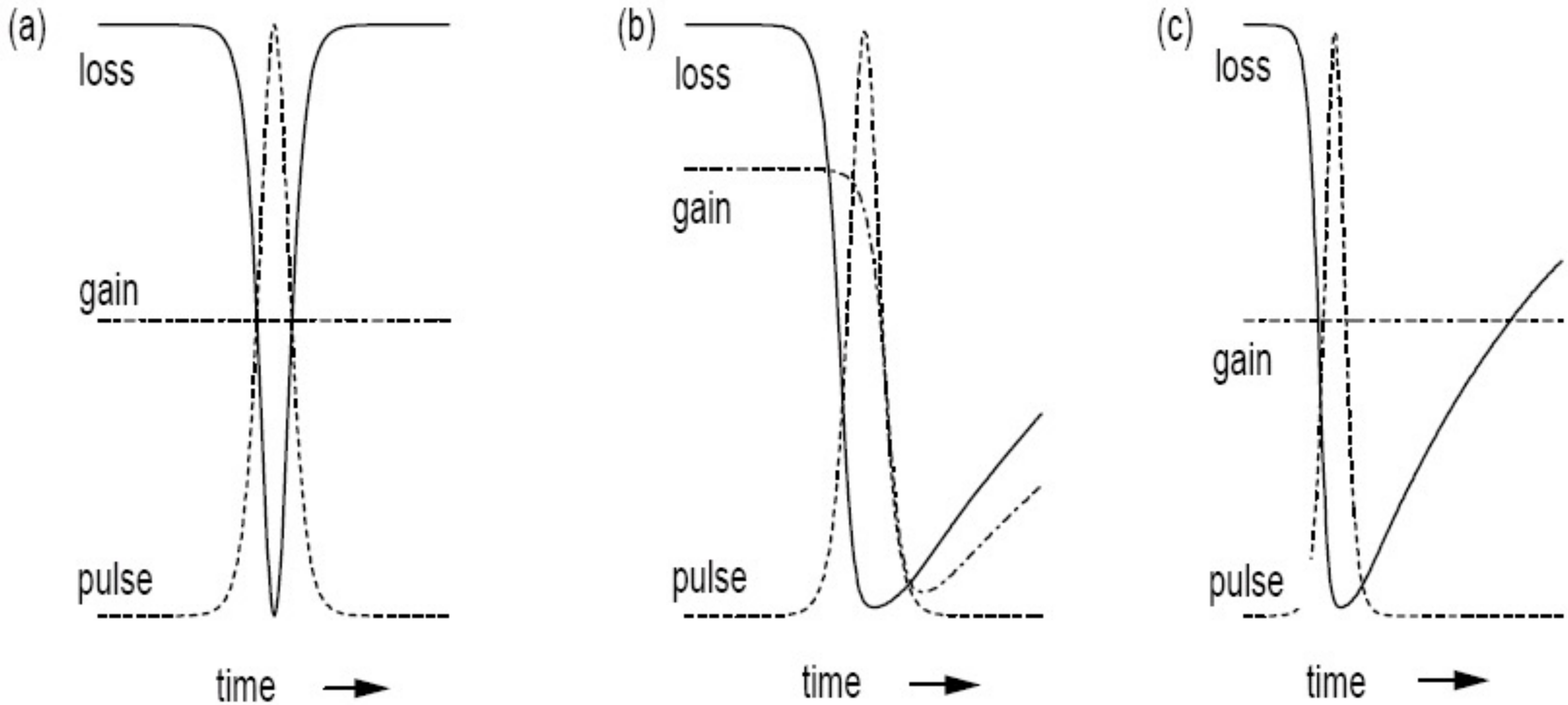


Fig. 6.1: Principles of mode locking

# 6.3 Soliton Mode Locking

$$T_R \frac{\partial A(T,t)}{\partial T} = \left[ g - l + (D_f + jD)\frac{\partial^2}{\partial t^2} - j\delta |A(T,t)|^2 - q(T,t) \right] A(T,t).$$

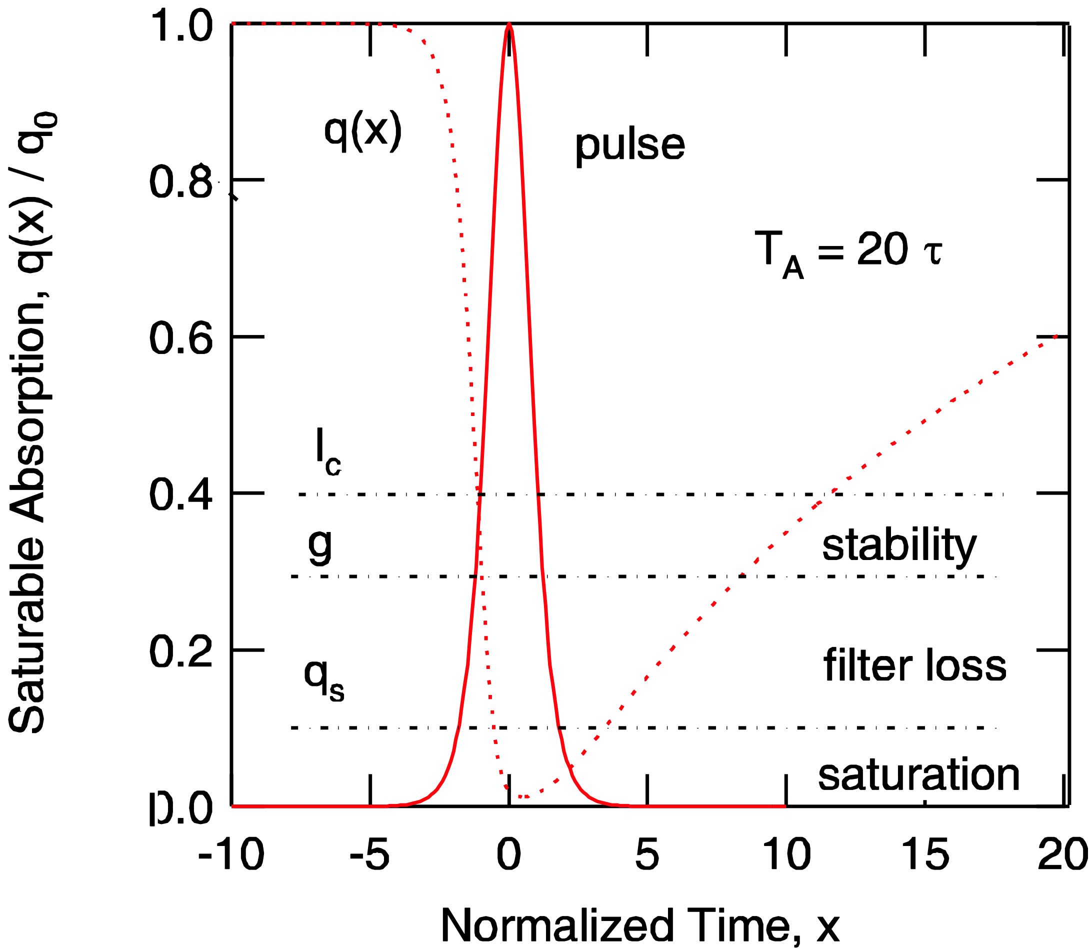


$$\frac{\partial q(T,t)}{\partial t} = -\frac{q - q_0}{\tau_A} - \frac{|A(T,t)|^2}{E_A}.$$

Fig. 6.7: Soliton modelocking

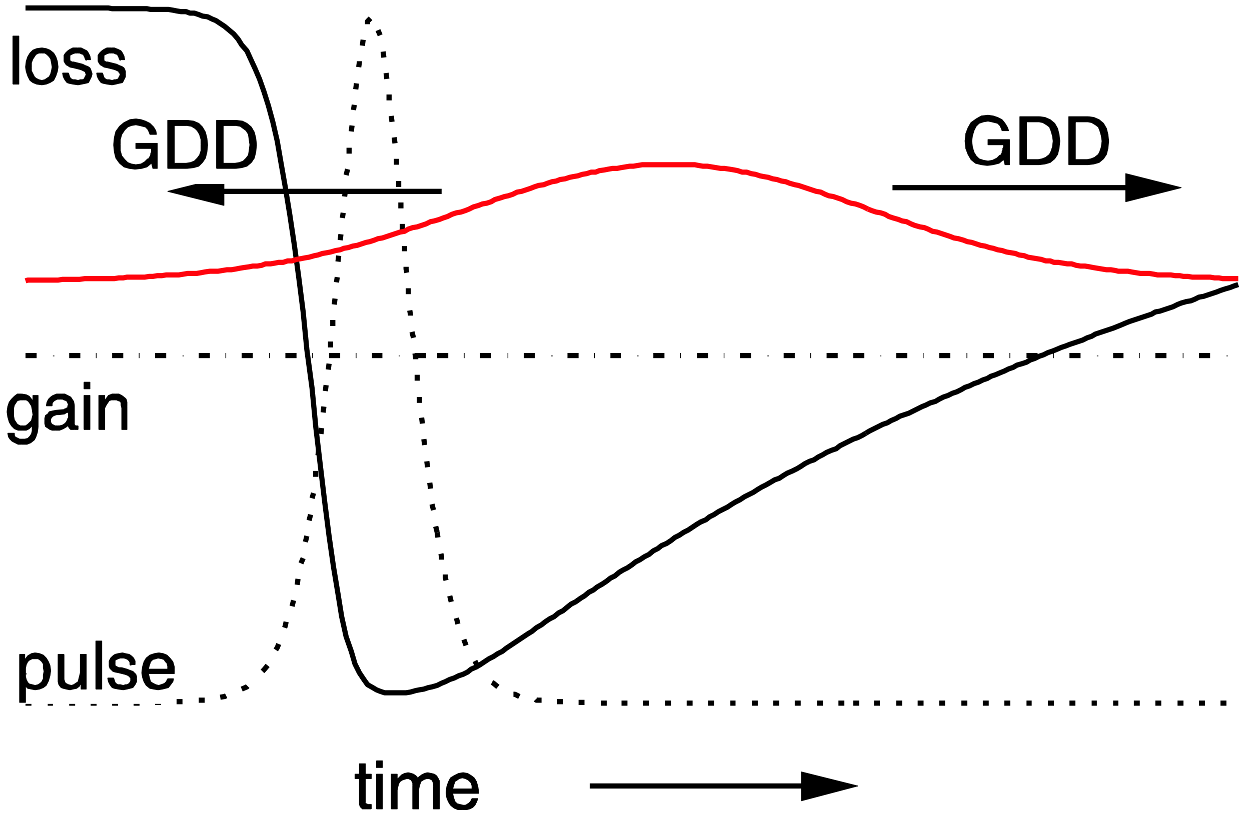


Fig. 6.8: Soliton Stability

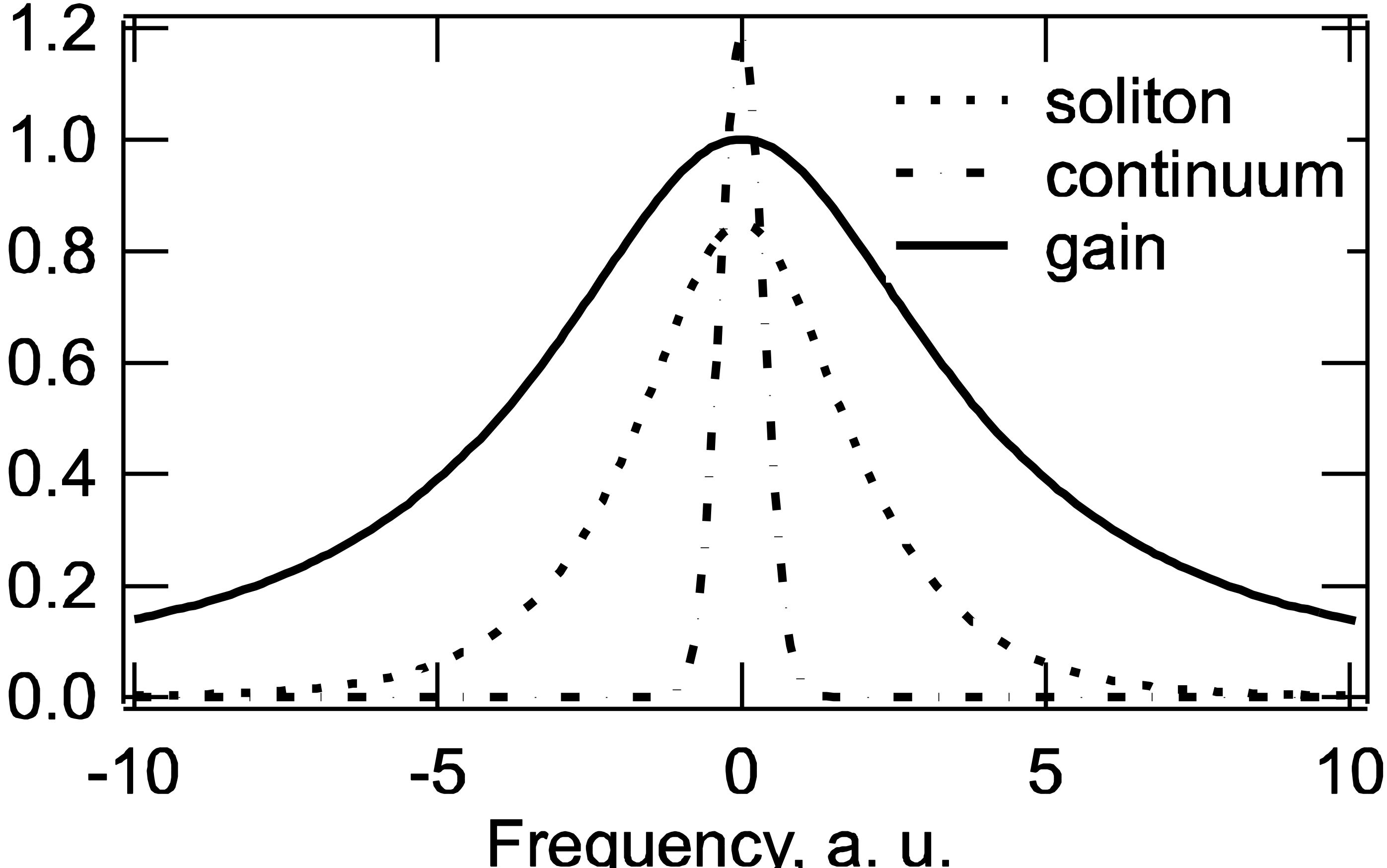


Fig. 6.9: Normalized gain, soliton and continuum.
The continuum is a long pulse exploiting the peak of the gain.

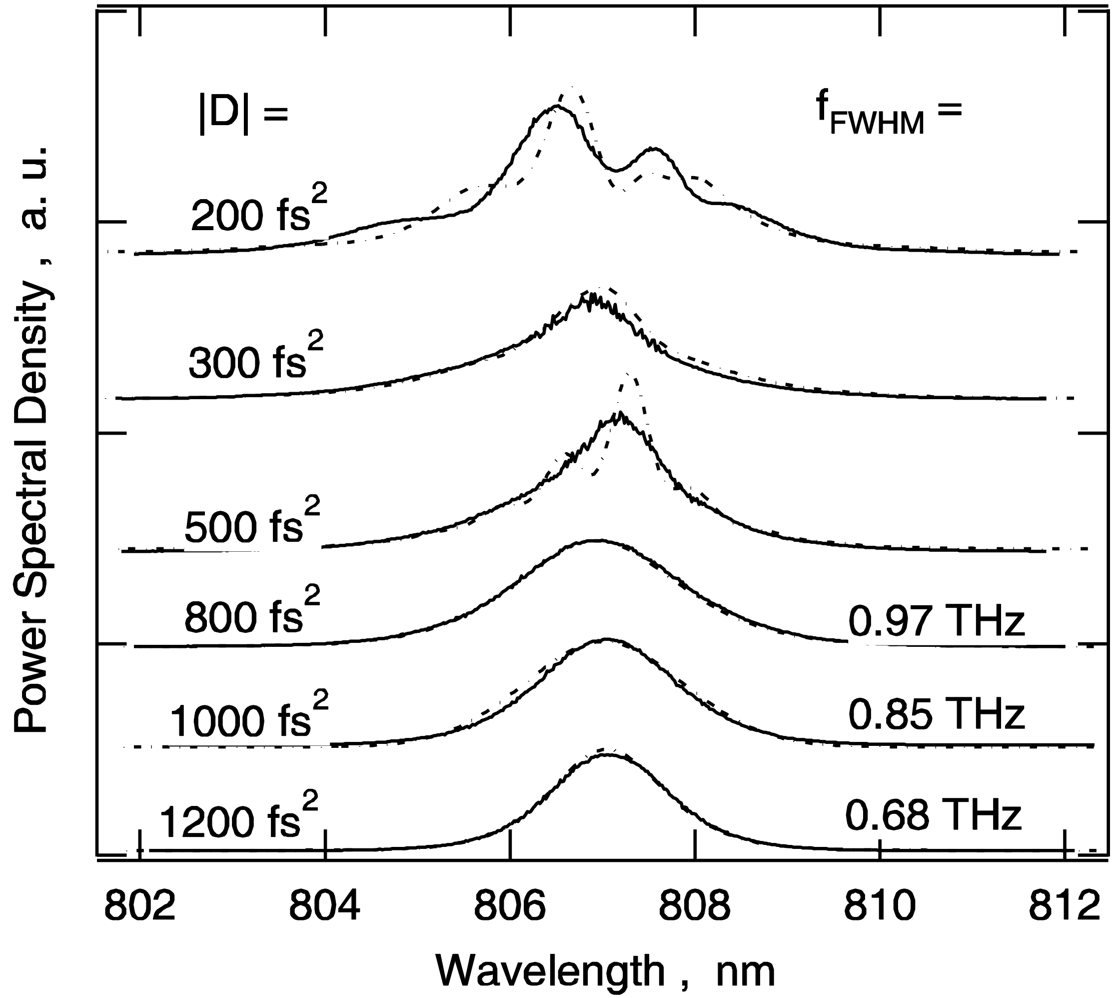


Fig. 6.10: Measured (---) and simulated (- - -) spectra from a semiconductor saturable absorber modelocked Ti:sapphire laser for different net intracavity dispersion.

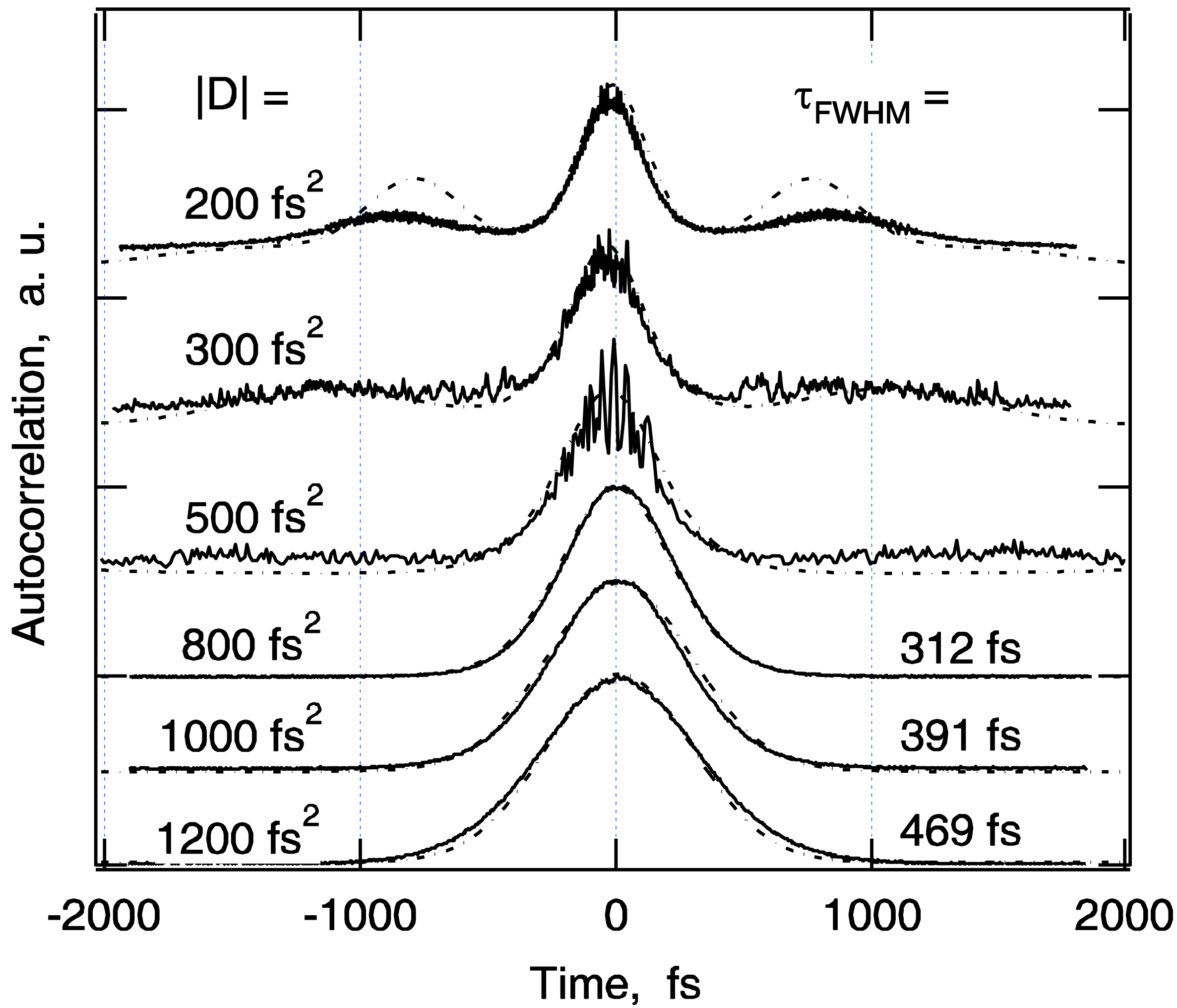


Fig. 6.11: Measured (----) and simulated (- - -) autocorrelations corresponding to the spectra shown in Figure 6.11

# 8 Semiconductor Saturable Absorbers

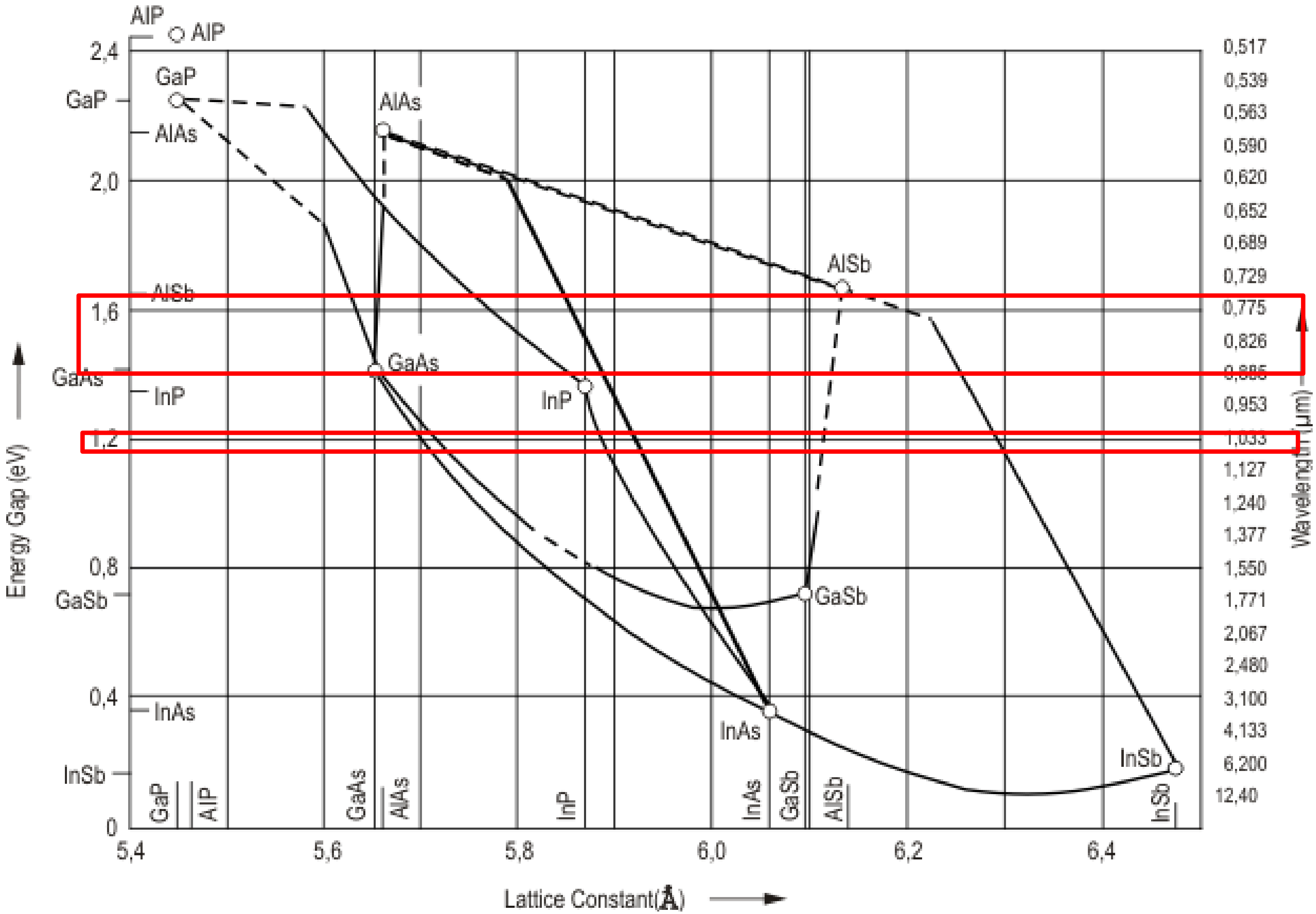


Fig. 8.1: Band Gap and lattice constant for various compound semiconductors. Dashed lines indicate ind. transitions.

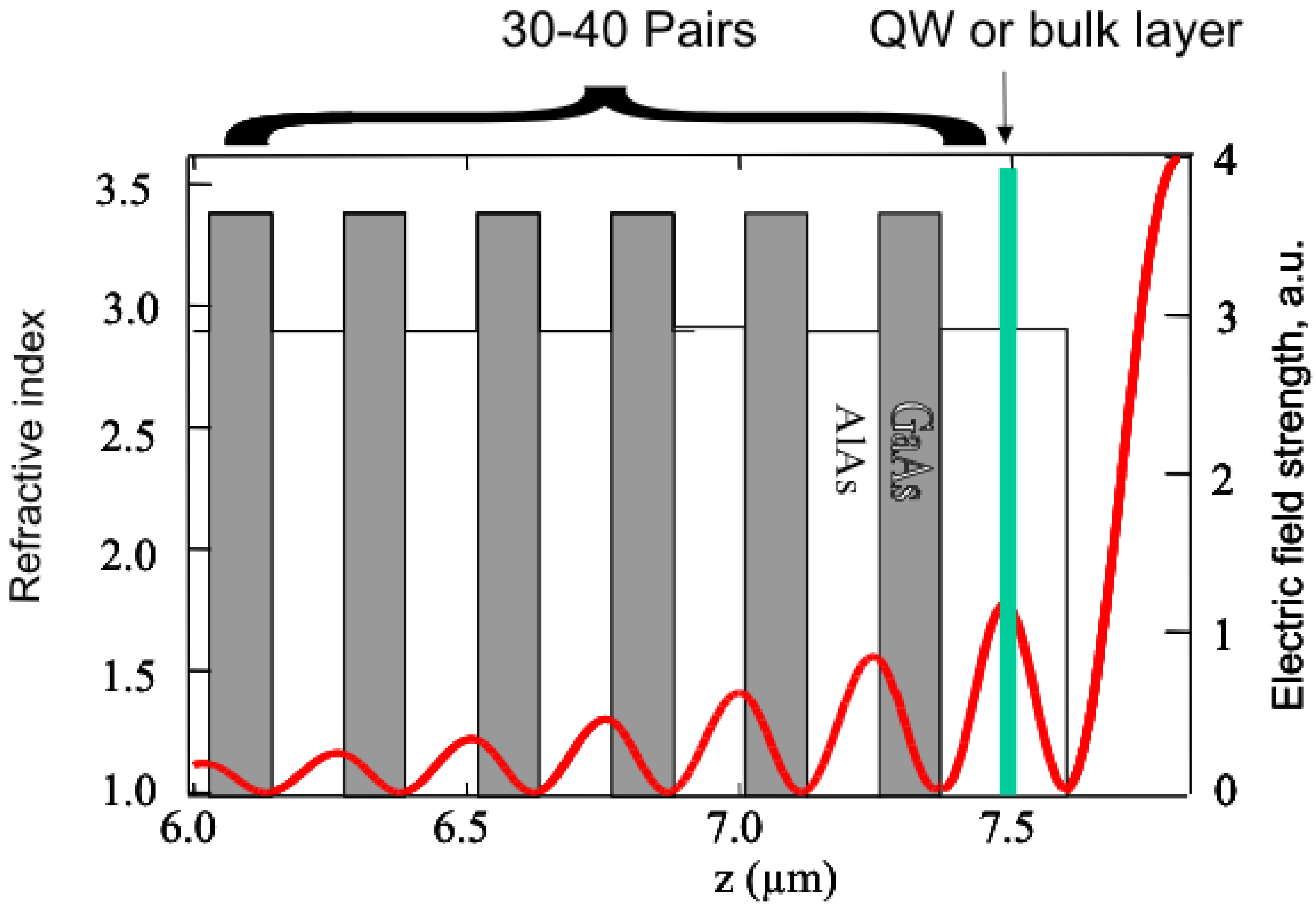


Fig. 8.2: Semiconductor saturable absorber mirror (SESAM)
or Semiconductor Bragg mirror (SBR)

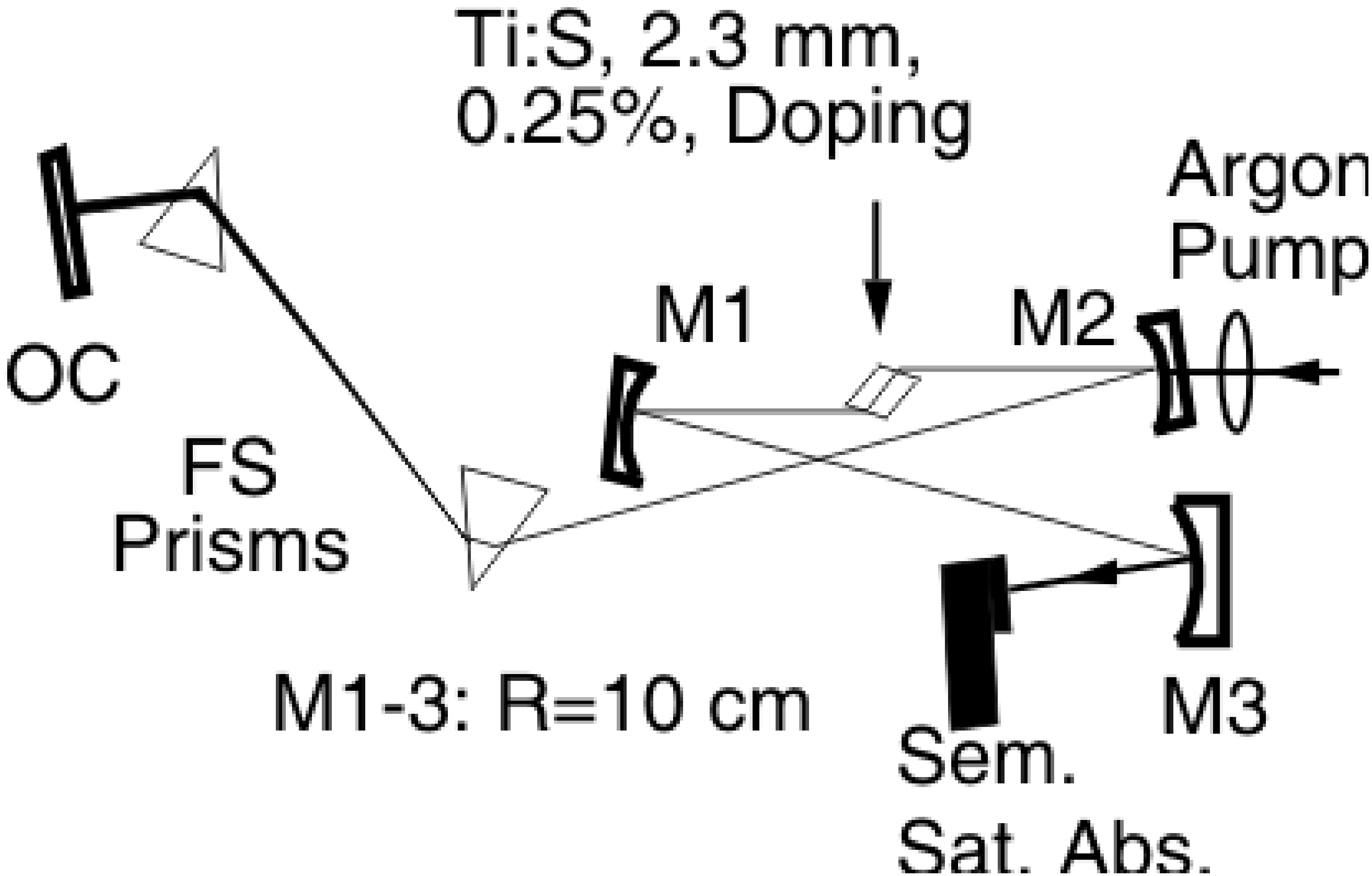


Fig. 8.3: Ti:sapphire laser modelocked by SBR

# 8.1 Carrier dynamics in semiconductors

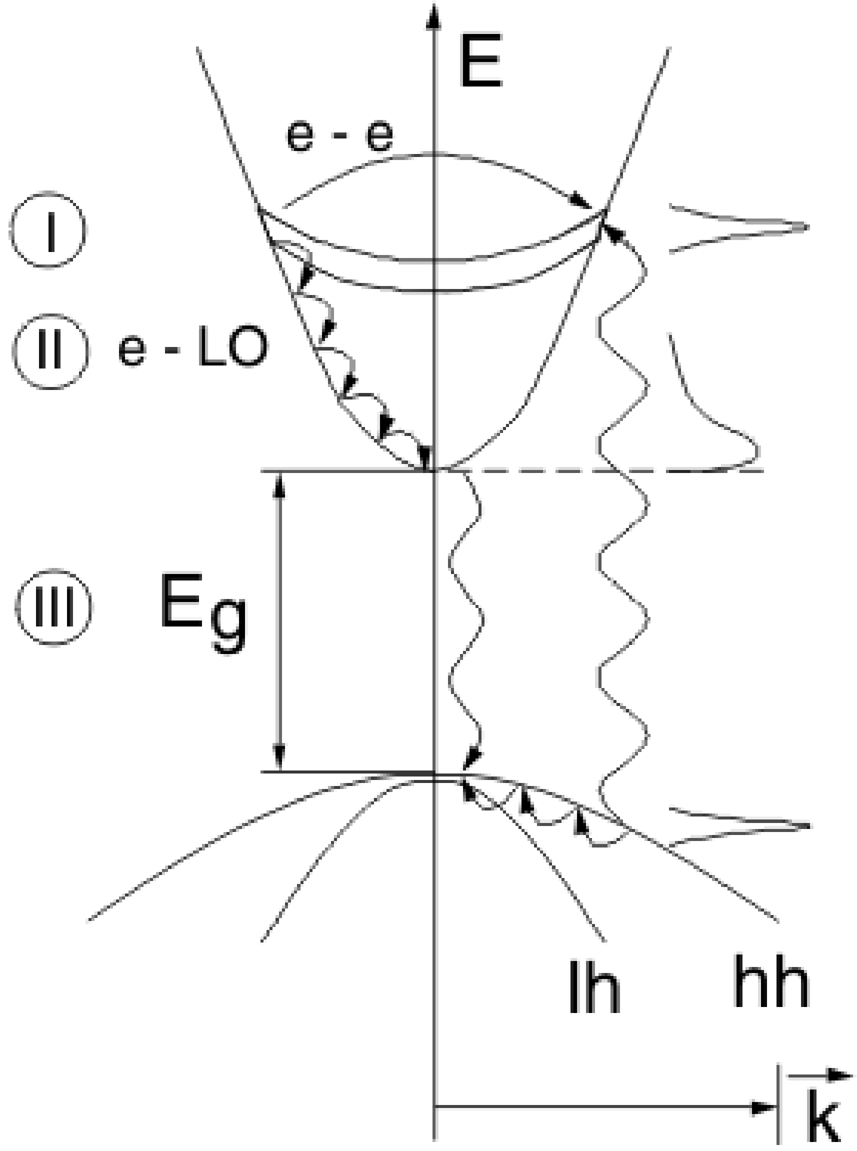


Table 8.4: Carrier dynamics in semiconductors

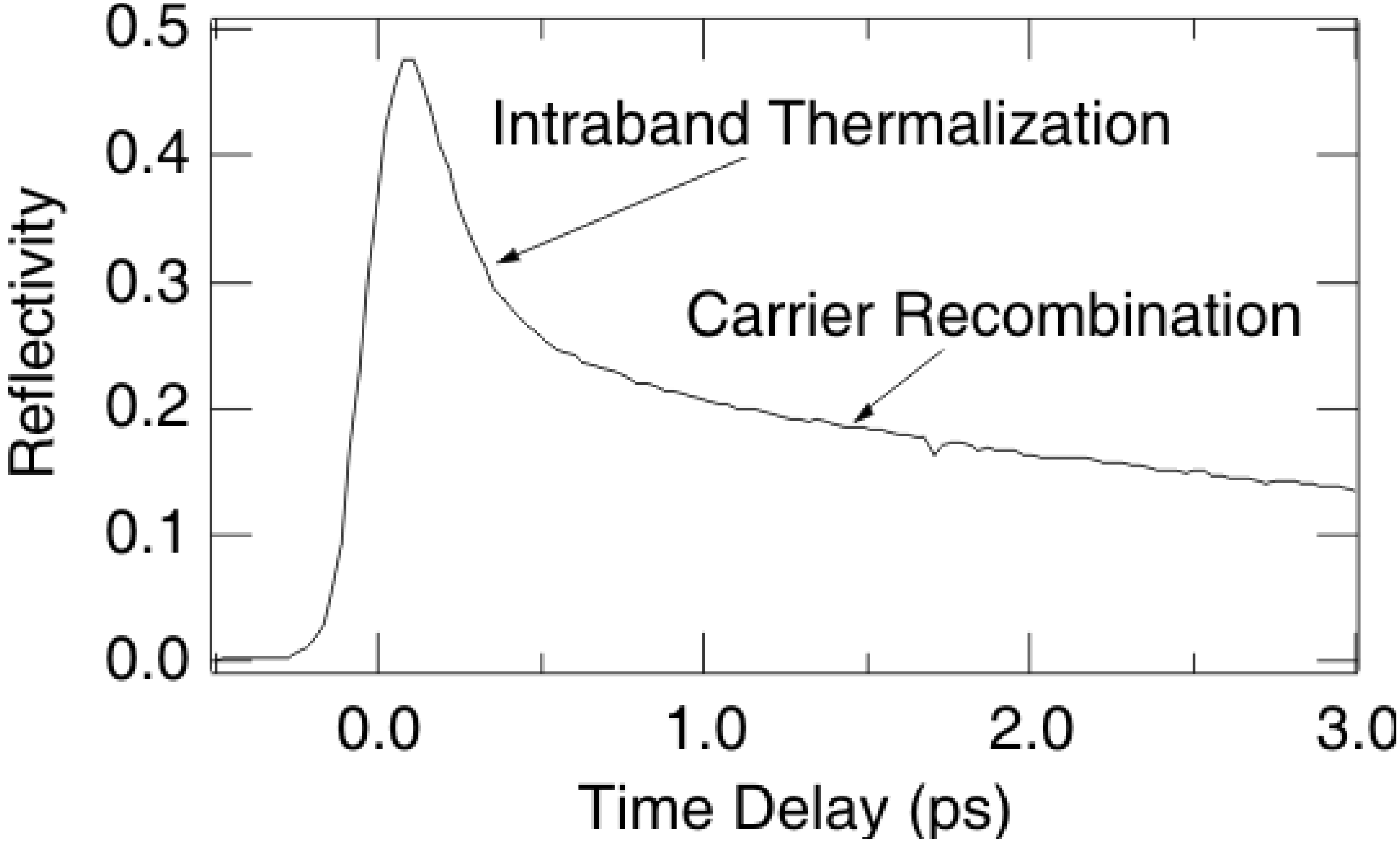


Fig. 8.5: Pump probe of a InGaAs multiple QW absorber

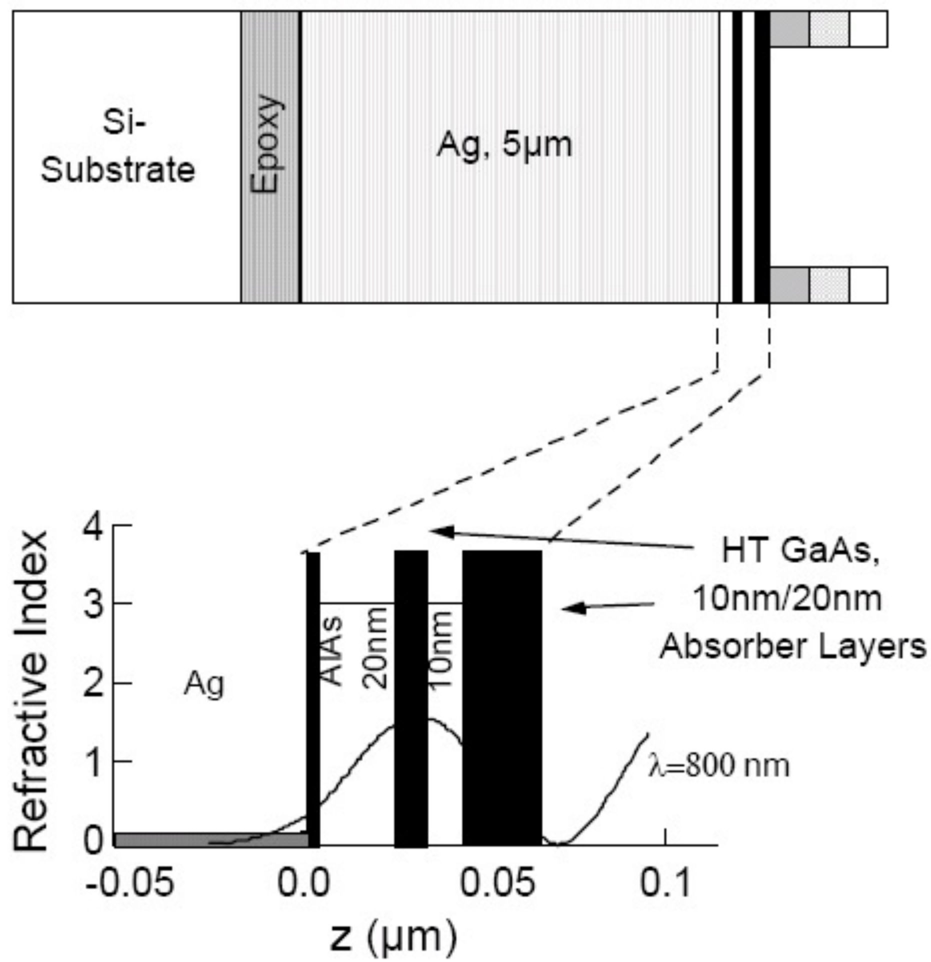


Fig. 8.7: GaAs saturable absorber on metal mirror

**Saturation fluence :**

$$d = 0.5 \text{ nm}$$

$$T_2 = 20 \text{ fs}$$

$$n_0 = 3$$

$$F_A = \frac{hf}{\sigma_A} = I_A \tau_A = \frac{\hbar^2}{2T_2 Z_F \left|\vec{M}\right|^2}$$

$$= \frac{\hbar^2 n_0}{2T_2 Z_{F0} \left|\vec{M}\right|^2} = 35\frac{\mu J}{cm^2}$$

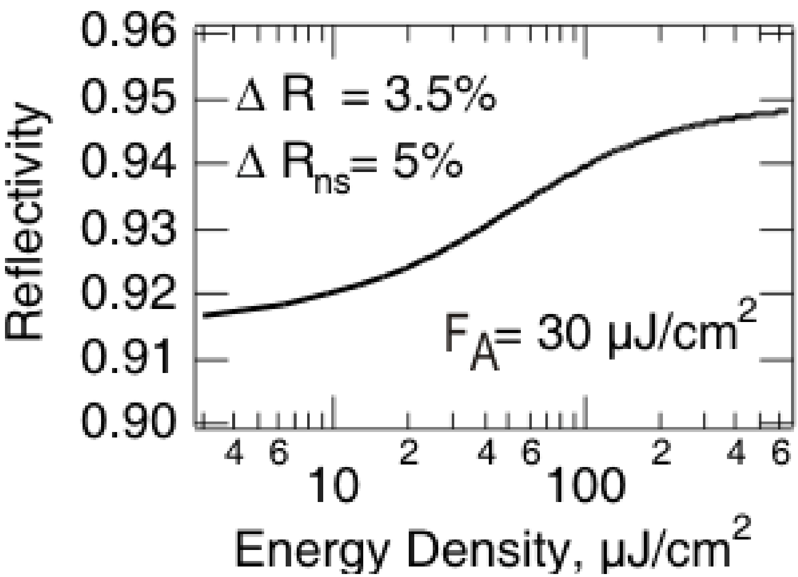


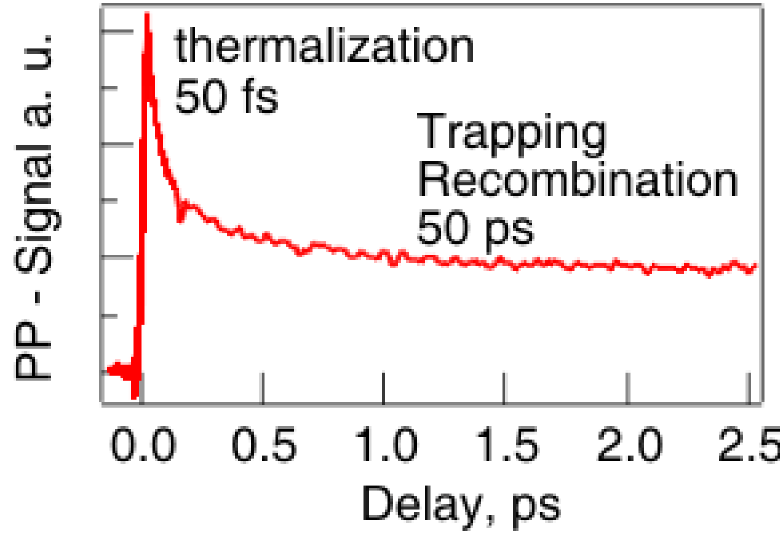


Fig. 8.6: Saturation fluence and pump probe measured with 10 fs pulses

# 8.2 High Fluence Effects

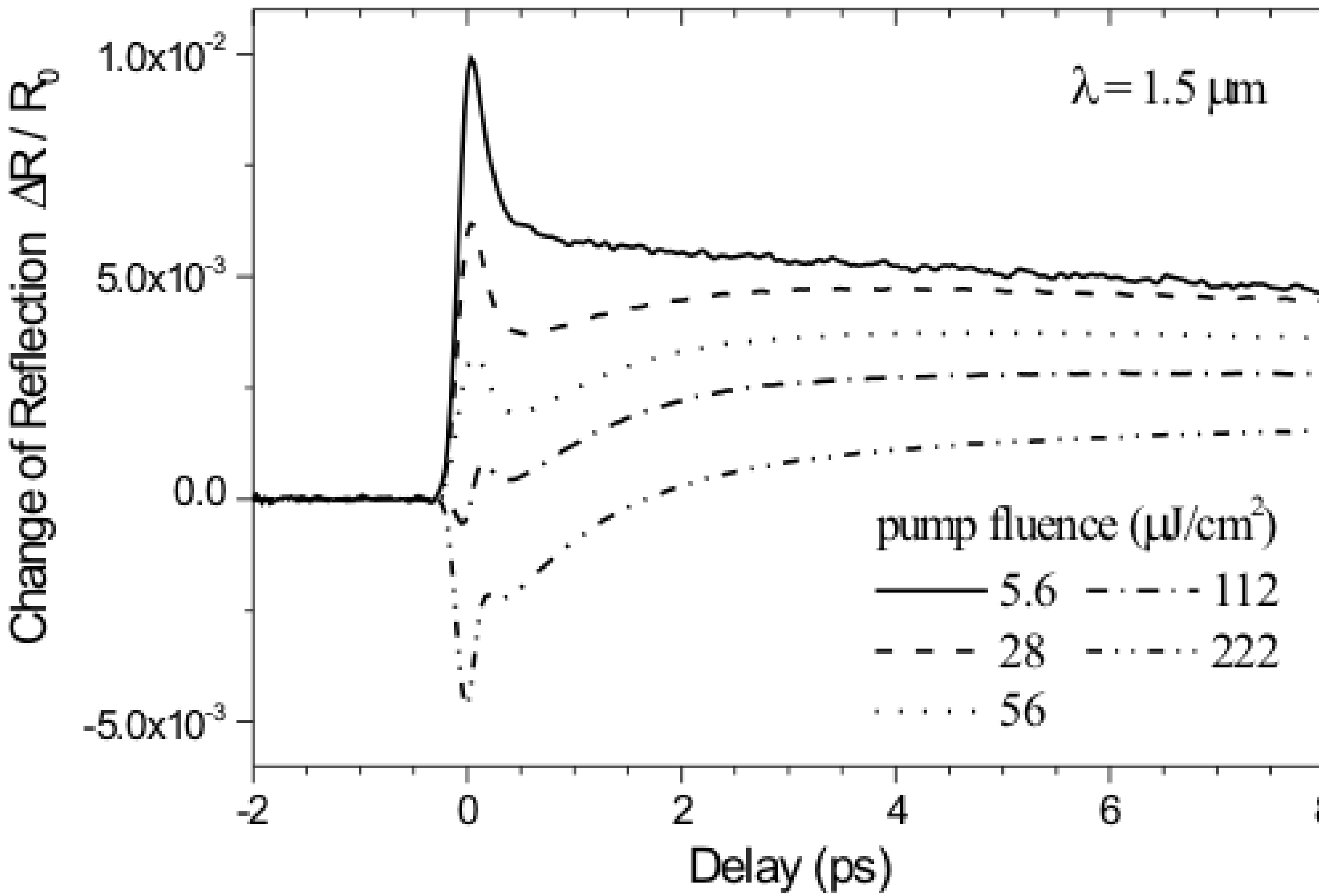


Fig. 8.8: Pump probe with low and high fluence

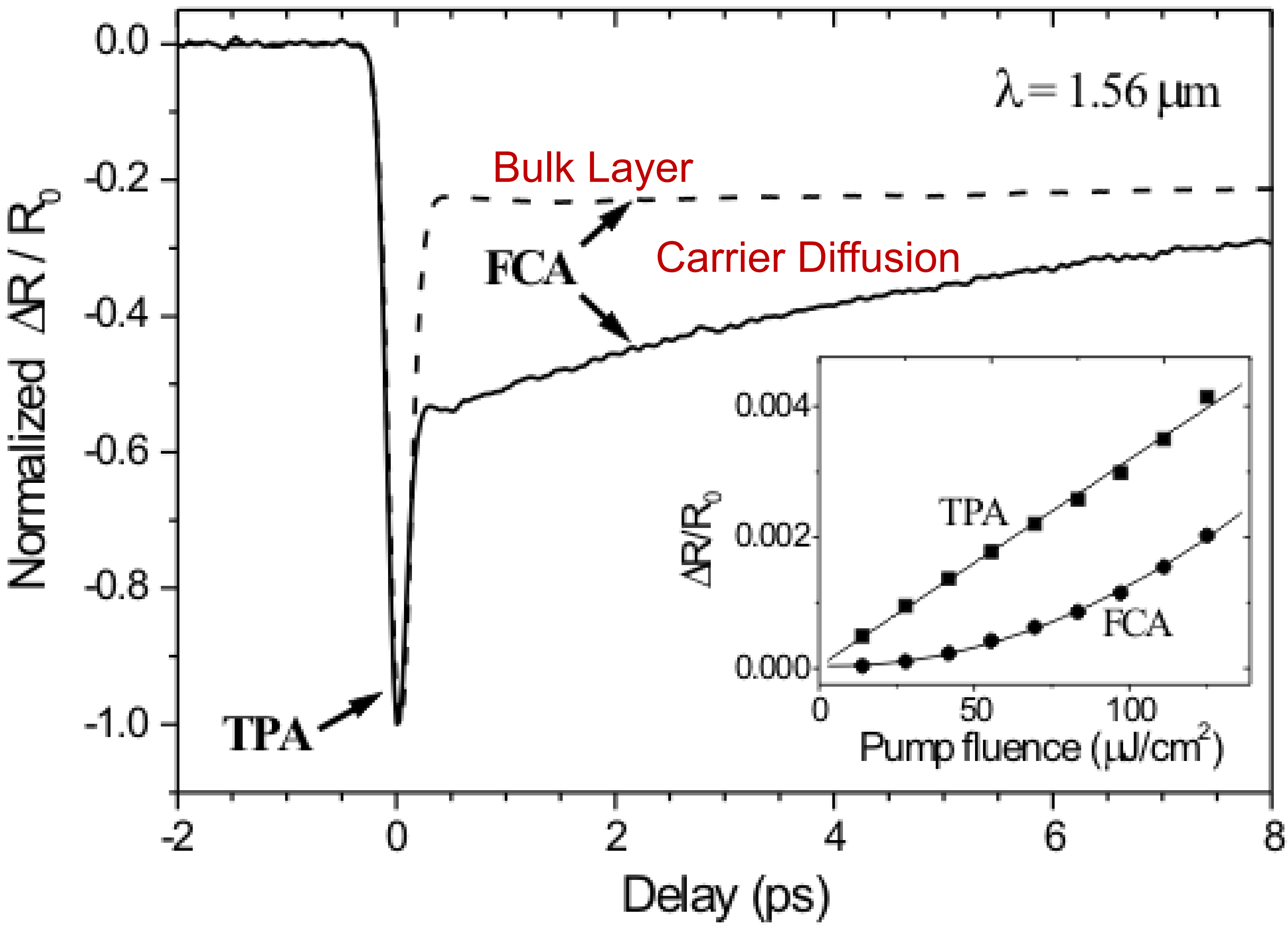


Fig. 8.9: TPA and FCA

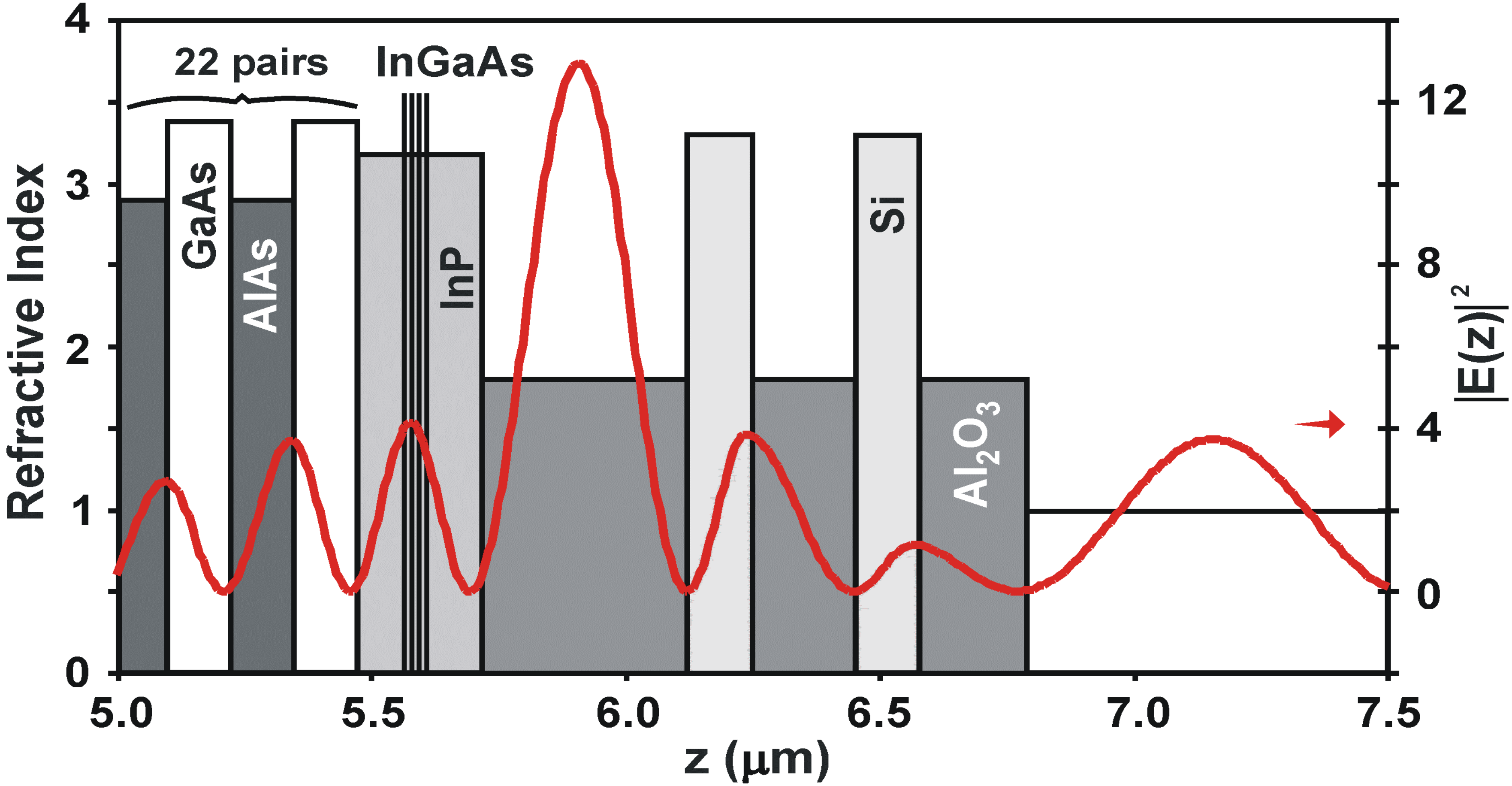


Fig. 8.10: Resonantly enhanced SBR

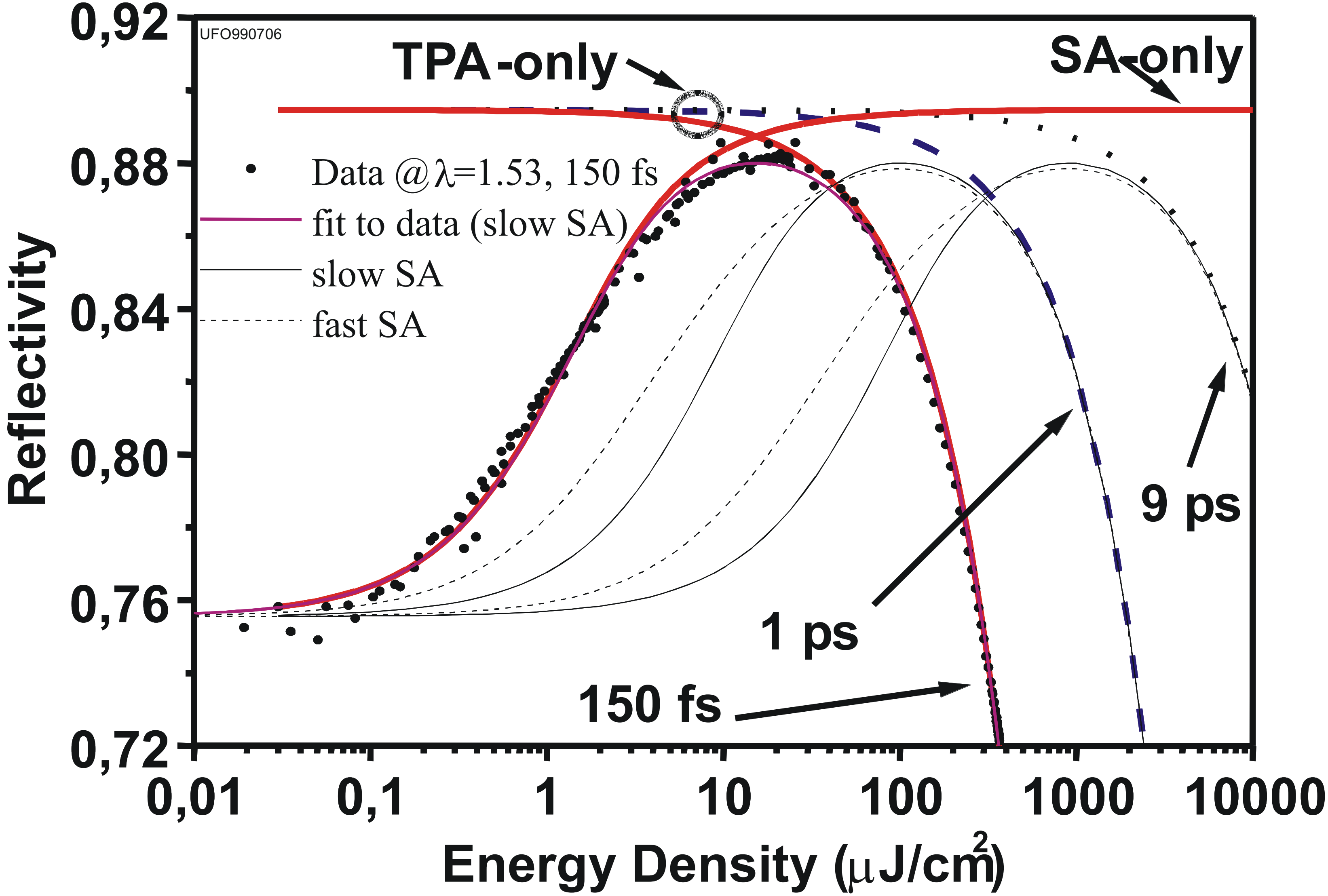


Fig. 8.11: Saturation fluence measurement of resonant absorber

# 8.3 Break-up into multiple pulses

$$l_m = \frac{D_f}{3\tau_m^2} + q_s(W_m)$$

$$l_1 = \frac{D_f}{3\tau_1^2} + q_s(W_1),$$

$$l_2 = \frac{D_f}{12\tau_1^2} + q_s(\frac{W_1}{2}).$$

$$\frac{D_f}{4\tau_1^2} < \Delta q_s(W) = q_s(\frac{W}{2}) - q_s(W)$$

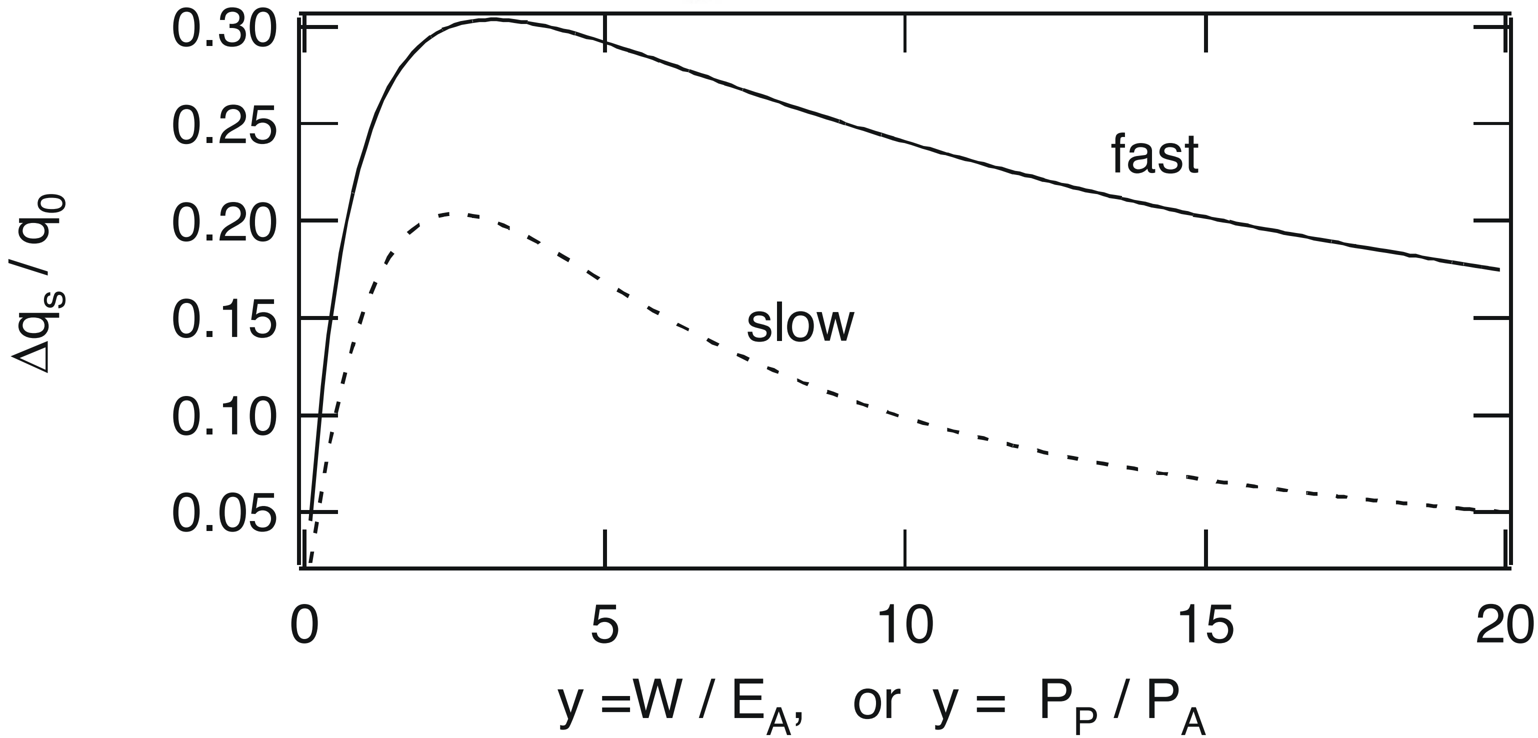


Fig. 8.12: Difference in loss experienced by a sech-shaped pulse in a slow (- - -) and a fast (_____) saturable absorber for a given pulse energy or peak power, respectively.

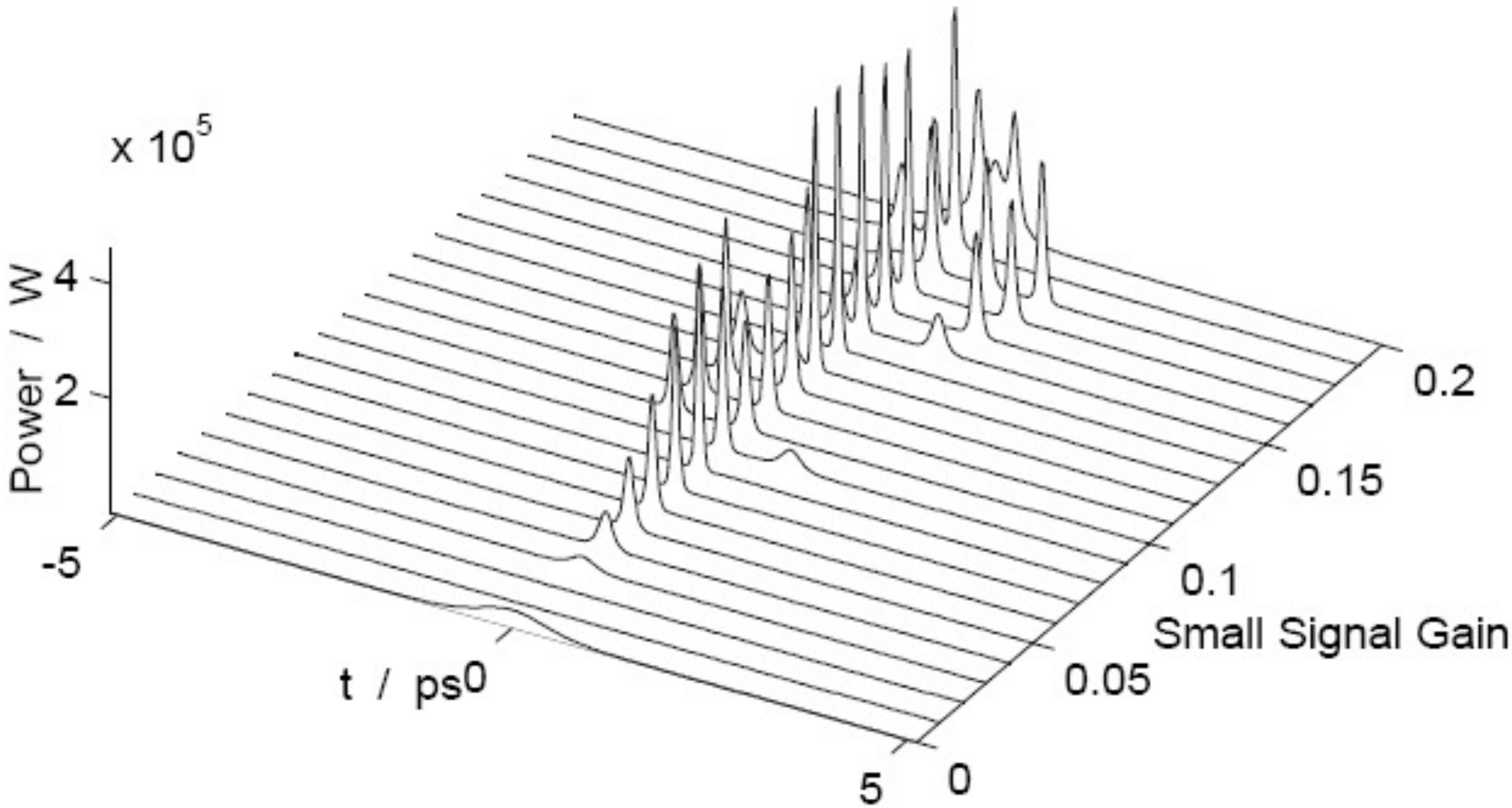


Fig. 8.13: Pulse intensity profiles after 20,000 round-trips each. Laser modelocked with sat. abs with recovery time $\tau_A$ = 200 fs.

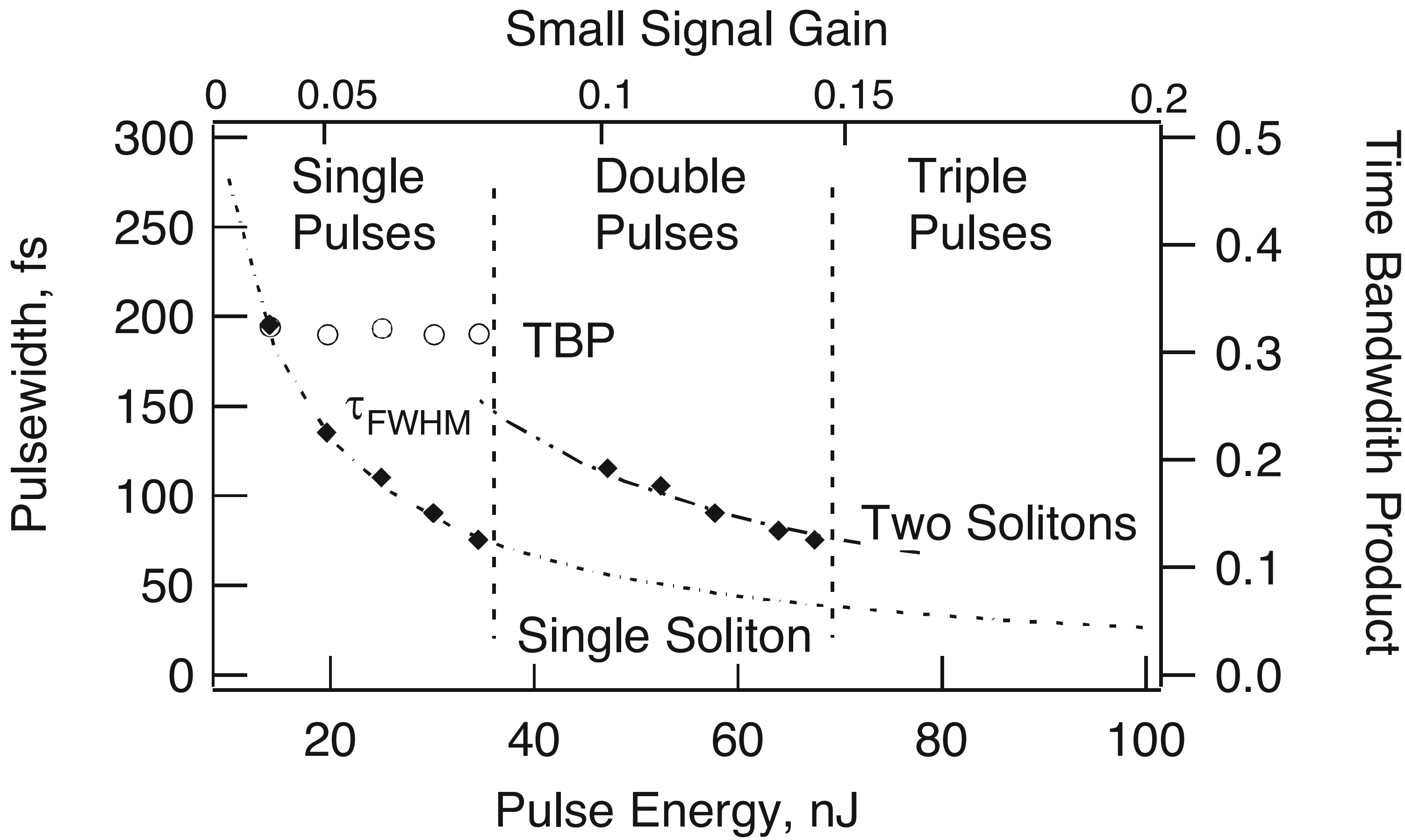


Fig. 8.14: Steady state pulse width and time-bandwidth product

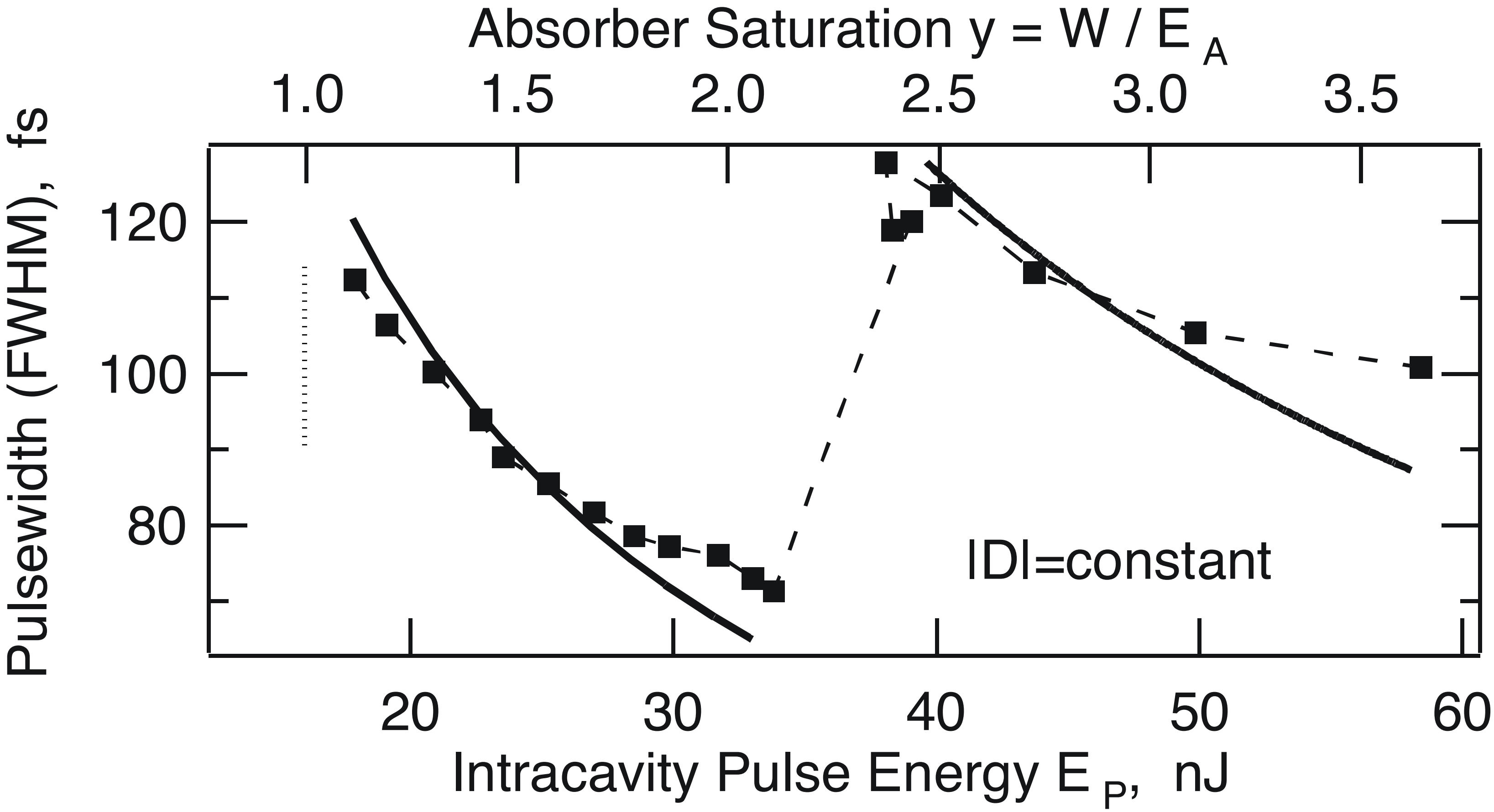


Fig. 8.15: Pulse width of Nd:glas laser.

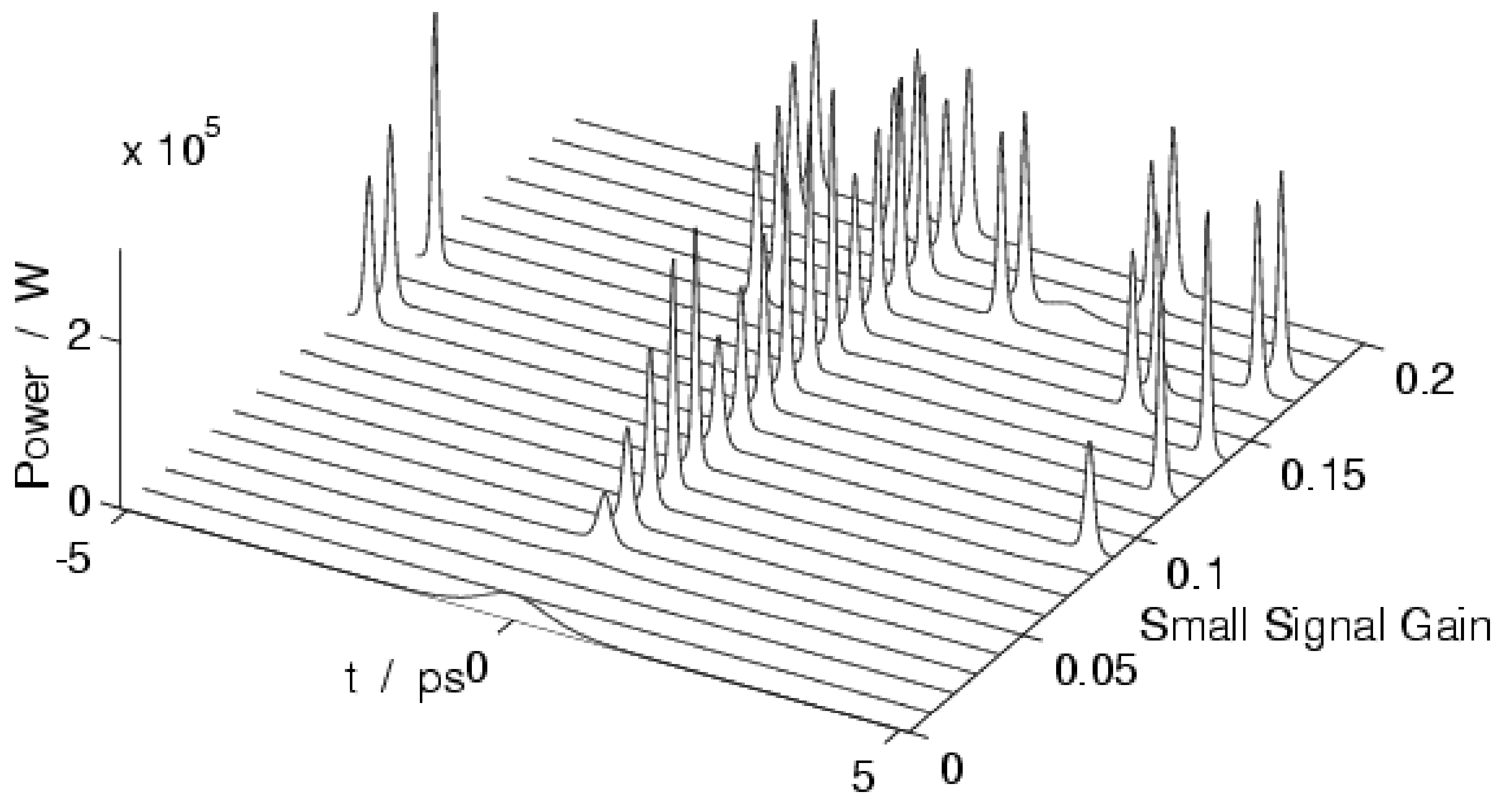


Fig. 8.16: Pulse intensity profiles after 20,000 round-trips each. Laser modelocked with sat. abs with shorter recovery time $\tau_A$ = 100 fs.